(Chairman). Carnegie Institution of Washington Publication, vol 87 (reprinted 1969)
53. Rothman DH (1985) Nonlinear inversion, statistical mechanics, and residual statics estimation. Geophysics 50:2784–2796
54. Rydelek P, Pujol J (2004) Real-Time Seismic Warning with a Two-Station Subarray. Bull Seism Soc Am 94:1546–1550
55. Sambridge M (1998) Exploring multi-dimensional landscapes without a map. Inverse Probl 14:427–440
56. Sambridge M (1999) Geophysical inversion with a Neighbourhood algorithm, vol I. Searching a parameter space. Geophys J Int 138:479–494
57. Sambridge M (1999) Geophysical inversion with a neighbourhood algorithm, vol II. Appraising the ensemble. Geophys J Int 138:727–746
58. Sambridge M (2003) Nonlinear inversion by direct search using the neighbourhood algorithm. In: International Handbook of Earthquake and Engineering Seismology, vol 81B. Academic Press, Amsterdam, pp 1635–1637
59. Sambridge M, Drijkoningen G (1992) Genetic algorithms in seismic waveform inversion. Geophys J Int 109:323–342
60. Sambridge M, Gallagher K (1993) Earthquake hypocenter location using genetic algorithms. Bull Seism Soc Am 83:1467–1491
61. Sambridge M, Kennett BLN (1986) A novel method of hypocentre location. Geophys J R Astron Soc 87:679–697
62. Sambridge M, Mosegaard K (2002) Monte Carlo Methods In Geophysical Inverse Problems. Rev Geophys 40:1009–1038
63. Satriano C, Lomax A, Zollo A (2007) Optimal, Real-time Earthquake Location for Early Warning. In: Gasparini P, Gaetano M, Jochen Z (eds) Earthquake Early Warning Systems. Springer, Berlin
64. Satriano C, Lomax A, Zollo A (2007) Real-time evolutionary earthquake location for seismic early warning. Bull Seism Soc Am 98:1482–1494
65. Sen M, Stoffa PL (1995) Global optimization methods in geophysical inversion. Elsevier, Amsterdam, p 281
66. Sethian JA (1999) Level set methods and fast marching methods. Cambridge University Press, Cambridge
67. Shannon CE (1948) A mathematical theory of communication. Bell Syst Tech J 27:379–423
68. Shearer PM (1994) Global seismic event detection using a matched filter on long-period seismograms. J Geophys Res 99:13,713–13,735
69. Shearer PM (1997) Improving local earthquake locations using the L1 norm and waveform cross correlation: Application to the Whittier Narrows, California, aftershock sequence. J Geophys Res 102:8269–8283
70. Steinberg DM, Rabinowitz N, Shimshoni Y, Mizrachi D (1995) Configuring a seismographic network for optimal monitoring of fault lines and multiple sources. Bull Seism Soc Am 85:1847–1857
71. Stummer P, Maurer HR, Green AG (2004) Experimental Design: Electrical resistivity data sets that provide optimum subsurface information. Geophysics 69:120–139
72. Tarantola A (1987) Inverse problem theory: Methods for data fitting and model parameter estimation. Elsevier, Amsterdam
73. Tarantola A (2005) Inverse Problem Theory and Methods for Model Parameter Estimation. SIAM, Philadephia
74. Tarantola A, Valette B (1982) Inverse problems = quest for information. J Geophys Res 50:159–170
75. Thurber CH, Kissling E (2000) Advances in travel-time calculations for three-dimensional strucutres. In: Thurber CH, Rabinowitz N (eds) Advances in Seismic Event Location. Kluwer, Amsterdam
76. Uhrhammer RA (1980) Analysis of small seismographic station networks. Bull Seism Soc Am 70:1369–1379
77. Um J, Thurber C (1987) A fast algorithm for two-point seismic ray tracing. Bull Seism Soc Am 77:972–986
78. van den Berg J, Curtis A, Trampert J (2003) Bayesian, nonlinear experimental design applied to simple, geophysical examples. Geophys J Int 55(2):411–421. Erratum: 2005. Geophys J Int 161(2):265
79. Vidale JE (1988) Finite-difference calculation of travel times. Bull Seism Soc Am 78:2062–2078
80. Winterfors E, Curtis A (2007) Survey and experimental design for nonlinear problems. Inverse Problems (submitted)
81. Wither M, Aster R, Young C (1999) An automated local and regional seismic event detection and location system using waveform correlation. Bull Seism Soc Am 8:657–669
82. Withers M, Aster R, Young C, Beiriger J, Harris M, Moore S, Trujillo J (1998) A comparison of select trigger algorithms for automated global seismic phase and event detection. Bull Seism Soc Am 88:95–106
83. Wittlinger G, Herquel G, Nakache T (1993) Earthquake location in strongly heterogeneous media. Geophys J Int 115:759–777
84. Zhou H (1994) Rapid 3-D hypocentral determination using a master station method. J Geophys Res 99:15439–15455

Books and Reviews

Gasparini P, Gaetano M, Jochen Z (eds) (2007) Earthquake Early Warning Systems. Springer, Berlin
Lee WHK, Stewart SW (1981) Principles and applications of microearthquake networks. Academic Press, New York
Thurber CH, Rabinowitz N (eds) (2000) Advances in Seismic Event Location. Kluwer, Amsterdam

Earthquake Magnitude

PETER BORMANN, JOACHIM SAUL
GeoForschungsZentrum Potsdam, Potsdam, Germany

Article Outline

Glossary

Technical terms that are written in the text in italics are explained in the Glossary.

Corner frequency The frequency f_c at which the curve that represents the Fourier amplitude spectrum of a recorded seismic signal abruptly changes its slope (see Fig. 5). For earthquakes, this frequency is related to the fault size, rupture velocity, rupture duration and stress drop at the source. Also the frequency at which the magnification curve of a recording system (e. g., Fig. 3) changes its slope.

Dispersion Frequency-dependence of the wave propagation velocity. Whereas seismic body-waves show virtually no dispersion, it is pronounced for seismic surface waves. It causes a significant stretching of the length of the surface-wave record and the rather late arrival of its largest amplitudes (Airy phases) from which the surface-wave magnitude M_S and the mantle magnitude M_m, respectively, are determined.

Earthquake size A frequently used, but not uniquely defined term. It may be related – more or less directly – to either the geometric-kinematic size of an earthquake in terms of area and slip of the fault or to the *seismic energy* radiated from a seismic source and its potential to cause damage and casualty (moment or energy *magnitude*).

Earthquake source In general terms, the whole area or volume of an *earthquake* rupture where seismic body waves are generated and radiated outwards. More specifically, one speaks either of the *source mechanism* or the source location. The latter is commonly given as earthquake hypocenter (i. e. the location at the source depth h from where the seismic rupture, collapse or explosion begins) or as the point on the Earth's surface vertically above the hypocenter, called the epicenter. Earthquakes at $h < 70$ km are shallow, those at larger depth either intermediate (up to $h = 300$ km) or deep earthquakes ($h = 300$–700 km). The determination of the geographical coordinates latitude φ, longitude λ, and focal depth h, is the prime task of seismic source location. However, for extended seismic sources, fault ruptures of great earthquakes in particular, the hypocenter is generally not the location of largest fault slip and/or seismic moment/energy release and the epicenter is then also not the location where the strongest ground shaking is felt. The locations of largest effects may be dozens of kilometers in space and many seconds to minutes in time away from the hypocenter or epicenter, respectively.

Fundamental modes The longest period oscillations of the whole Earth with periods of about 20 min (spheroidal mode), 44 min. (toroidal mode) and some 54 min ("rugby" mode), excited by great earthquakes.

Magnitude A number that characterizes the relative *earthquake size*. It is usually based on measurement of the maximum motion recorded by a seismograph (sometimes for waves of a particular type and frequency) and corrected for the decay of amplitudes with epicenter distance and source depth due to geometric spreading and attenuation during wave propagation. Several magnitude scales have been defined. Some of them show *saturation*. In contrast, the moment magnitude (M_w), based on the concept of *seismic moment*, is uniformly applicable to all earthquake sizes but is more difficult to compute than the other types, similarly the energy magnitude, M_e, which is based on direct calculation of the *seismic energy* E_s from broadband seismic records.

Saturation (of magnitudes) Underestimation of *magnitude* when the duration of the earthquake rupture significantly exceeds the seismic wave period at which the magnitude is measured. The shorter this period, the earlier respective magnitudes will saturate (see relation (13) and Figs. 4 and 5).

Seismic energy Elastic energy E_s (in joule) generated by, and radiated from, a seismic source in the form of seismic waves. The amount of E_s is generally much smaller than the energy associated with the non-elastic deformation in the seismic source (see *seismic moment* M_o). The ratio $E_s/M_o = (\Delta\sigma/2\mu) = \tau_a/\mu$, i. e., the seismic energy released per unit of M_o, varies for earthquakes in a very wide range between some 10^{-6} and 10^{-3}, depending on the geologic-tectonic environment, type of *source mechanism* and related stress drop $\Delta\sigma$ or apparent stress τ_a.

Seismic moment M_o A special measure of earthquake size. The moment tensor of a shear rupture (see *earthquake source*) has two non-zero eigenvalues of the amount $M_o = \mu \bar{D} F_a$ with μ-shear modulus of the ruptured medium, $\bar{D}$-average source dislocation and F_a-area of the ruptured fault plane. M_o is called the scalar seismic moment. It has the dimension of Newton meter (Nm) and describes the total non-elastic (i. e., ruptural and plastic) deformation in the seismic source volume. Knowing M_o, the moment *magnitude* M_w can be determined via Eq. (11).

Source mechanism Depending on the orientation of the earthquake fault plane and slip direction in space, one discerns different source mechanisms. Strike-slip faults are vertical (or nearly vertical) fractures along

which rock masses have mostly shifted horizontally. Dip-slip faults are inclined fractures. If the rock mass above an inclined fault moves down (due to lateral extension) the fault is termed normal, whereas, if the rock above the fault moves up (due to lateral compression), the fault is termed reverse (or thrust). Oblique-slip faults have significant components of both slip styles (i. e., strike-slip and dip-slip). The greatest earthquakes with the largest release of seismic moment and the greatest potential for generating tsunamis are thrust faults in subduction zones where two of Earth's lithosphere plates (e. g., ocean–continent or continent–continent) collide and one of the two plates is subducted underneath the overriding plate down into the Earth's mantle. Different source mechanisms are characterized by different radiation patterns of seismic wave energy.

Transfer function The transfer function of a seismic sensor-recorder system (or of the Earth medium through which seismic waves propagate) describes the frequency-dependent amplification, damping and phase distortion of seismic signals by a specific sensor-recorder (or medium). The modulus (absolute value) of the transfer function is termed the amplitude-frequency response or, in the case of seismographs, also magnification curve (see Fig. 3).

Definition of the Subject

Besides earthquake location (i. e., the determination of the geographical coordinates of the epicenter, the hypocenter depth and the origin time; for definition of these terms see *earthquake source* in the Glossary), the *magnitude* is the most frequently determined and commonly used parameter to characterize an earthquake. Despite its various imperfections, it provides important information concerning the earthquake source spectrum at the period where the magnitude is measured and current source theories (cf. [3]) allow one to understand differences in the source spectra of different earthquakes in terms of source dimension and stress drop, i. e., the difference between the stress level before and after the earthquake. Via various empirical relations, magnitudes enable estimates of the *seismic moment* and the *seismic energy* released by the earthquake. These parameters are important in the discussion of various global problems such as the seismic slip rates between lithosphere plates and the excitation of Chandler Wobble [25]. Besides these more academic issues, magnitude values have an immense practical value in providing:

a) Rapid simple parameter estimates of the strength of an earthquake that can help to realistically assess the related ground shaking or tsunami potential and thus assist efficient disaster management response;
b) Mass data in earthquake catalogs and data banks, covering long time periods over many decades – and hopefully centuries in future, which allows one to assess the seismic activity and related hazards of Earth's regions and their possible variability in space and time. This is not only of high scientific interest, but also the very basis for realistic long-term disaster preparedness and risk mitigation efforts.

The term magnitude and the basic method of its determination were introduced by Charles F. Richter in 1935 [71]. He intended to compare the relative *earthquake size* in southern California in terms of differences in the maximum amplitudes A recorded at a network of seismic stations that were equipped with standard short-period Wood–Anderson (WA) torsion seismometers.

The WA seismometer response is depicted in Fig. 3 and Fig. 1 shows a WA record and magnitude measurement example. In order to make amplitudes recorded by stations at different epicentral distances D from the earthquake comparable, Richter had to compensate for the amplitude decay with D using an appropriate correction term $-A_o(D)$. Since the strength and thus the radiated amplitudes of earthquakes vary in a wide range Richter defined his local magnitude scale M_L, determined from records at source distances up to 600 km, as follows:

> "*The magnitude of any shock is taken as the logarithm of the maximum trace amplitude, expressed in microns, with which the standard short-period torsion seismometer … would register that shock at an epicentral distance of 100 km.*"

Thus:

$$M_L = \log A_{max} - \log A_o(D) \; . \tag{1}$$

According to the above definition, an amplitude of 1 μm in a WA record at a distance $D = 100$ km from the epicenter would correspond to $M_L = 0$. Amplitude means in (1) and the following text either the center-to-peak or half of the peak-to-trough amplitude.

Wood–Anderson (WA) seismographs record horizontal short-period ground motions with an amplification of only about 2080 times [82]. Modern electronic seismographs may achieve magnifications larger than 10^6 and thus are able to record local earthquakes with even negative magnitudes, down to about -2. The largest values determined with the M_L scale are around seven. Later it was found that all magnitudes derived from short-period waves (typically with periods $T < 3$ s) show *saturation*

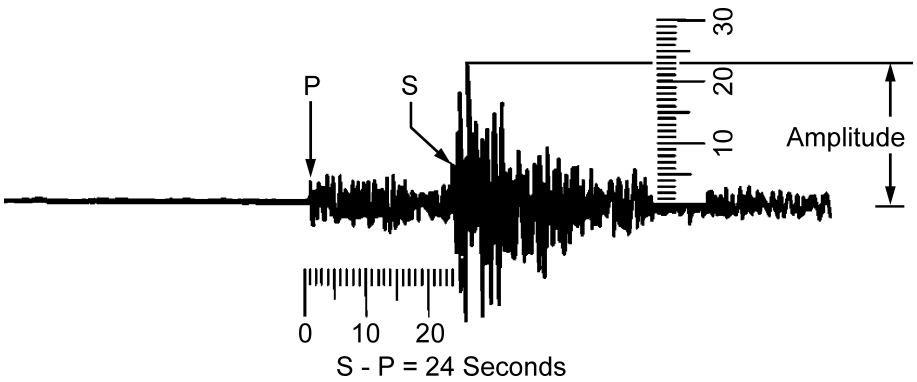

Earthquake Magnitude, Figure 1
Record of a short-period Wood–Anderson seismograph (frequency-magnification curve see Fig. 3) of a local earthquake. *P* marks the onset of the first arriving longitudinal *P* wave, and *S* the onset of the much stronger secondary, transverse polarized shear wave. Note the long tail of coda-waves following *S*. From the time difference $S - P = 24$ s follows a hypocentral distance $R = 190$ km. The maximum record amplitude is $A_{max} = 23$ mm. Applying the amplitude-distance correction $-\log A_o(190\,\text{km}) = 3.45$ according to Richter [72] results in a magnitude $M_L = 4.8$

(see Glossary, Fig. 4 and Sect. "Magnitude Saturation and Biases Due to Earthquake Complexity"). Therefore, it was necessary to develop complementary magnitude scales that use medium to long-period ($T \approx 5\,\text{s} - 30\,\text{s}$) as well as very long-period waves ($T \approx 50\,\text{s} - 3000\,\text{s}$) in order to enable less or non-saturating magnitude estimates (see Sect. "Introduction to Common Magnitude Scales: Potential and Limitations"). For the so far strongest instrumentally recorded earthquake (Chile 1960) a value of $M = 9.5$ was determined that way. Accordingly, instrumental seismic monitoring currently covers the magnitude range of about $-2 \leqslant M < 10$. This roughly corresponds to ruptures of some millimeters to more than 1000 km long. They radiate approximately the same amount of seismic wave energy E_s as well-contained underground explosions with yields ranging from a few milligrams (10^{-9} t) to several 10 to 100 Gt (1 Gt $= 10^9$ t) Trinitrotoluol (TNT) equivalent, thus covering about 20 orders in energy. Earthquakes with magnitudes around four may cause only minor local damage, those with magnitudes > 6 heavy damage, and those with magnitudes > 7 already widespread devastating damage. Shallow submarine earthquakes with magnitudes > 7 may generate significant local tsunamis with damage potential to nearby shores whereas those with magnitudes > 8.5 may stimulate ocean-wide tsunamis causing destruction and casualties even at shores thousands of kilometers away from such earthquakes.

In order to measure and classify *earthquake size* in the wide range of magnitudes from about -2 to < 10 and satisfy specific requirements in research and application which are based on magnitude data, it was indispensable to develop different magnitude scales that are complementary, but properly scaled to the original Richter M_L. Thus, there exists today a host of magnitude scales applicable in a wide range of source distances from less than 1 km up to more than 10,000 km. These scales, their specifics, potential and limitations are discussed in detail (with many reference given) in Chapter 3 of the IASPEI New Manual of Seismological Observatory Practice [6]. The early pioneers of magnitude scales, Beno Gutenberg and Charles Richter, had hoped that different magnitude scales could be cross-calibrated to yield a unique value for any given earthquake (cf. [25,30]. In their joint book [29] "Seismicity of the Earth" (1954; first edition 1949) and later in Richter's [72] famous text book "Elementary Seismology" as well as in Duda [22] only one magnitude value M was given per earthquake. However, this approach proved only partially realistic under certain conditions and within limited magnitude ranges because of the often significant differences in measurement procedures as well as period and bandwidth ranges used in later magnitudes scales. Decades later it took significant efforts (cf. [1,2,25]) to reconvert these M values, which turned out to be not even compatible (cf. [25]) into their original body or surface wave magnitudes in order to get values that agree with the original definition of these specific magnitude scales and can be compared with current data of the same type.

In general, such magnitude conversion relations strongly depend on initial data errors and the type of least-square regression procedure applied [11,14]. Moreover, the latter have often not been interpreted and used in a correct way. This may result in the case of noisy mag-

nitude data for events at the upper and lower end of the investigated magnitude range, in conversion errors of more than 0.5 magnitude units (m.u.) with serious consequences on seismic hazard estimates based on such converted magnitudes (cf. [7,11,14,15]). Moreover, magnitude values determined within the *saturation* range of a given scale cannot reliably be converted via empirical regression relations into the equivalent magnitude values of another less or non-saturating magnitude scale (see Fig. 4 and [44]). Furthermore, some magnitudes relate best to the released *seismic energy* while others are scaled to the static *seismic moment*, i. e., they measure equally important but fundamentally different physical aspects of the source and the radiated seismic waves and may differ by sometimes more than 1 m.u. Thus there is no way to characterize *earthquake size* in all its different aspects by just a single magnitude value. Proper interpretation and use of different types of magnitude data, however, requires one to understand the physics behind such values and how these may be affected by the complexity and duration of the earthquake rupture process. Further, this necessitates one to discriminate unambiguously the different types of magnitude values by using a unique nomenclature and to assure that magnitude values published with a given nomenclature have been determined with an internationally agreed standard procedure. With this in mind, the most important magnitude scales and related problems are summarized in Sects. "Introduction to Common Magnitude Scales: Potential and Limitations" and "Common Magnitude Estimates for the Sumatra 2004 M_w 9.3 Earthquake".

Introduction to Common Magnitude Scales: Potential and Limitations

Magnitude Scales Used in the Local and Regional Distance Range ($D < 2000$ km)

The original Richter local magnitude scale for Southern California [71] has been further developed since its invention [38]. In its expanded form (with the nomenclature M_L common in the United States), the following relation now holds:

$$M_L = \log_{10}(A_{max}) + 1.11 \log_{10} R + 0.00189\, R - 2.09 \quad (2)$$

with R = distance from the station to the hypocenter in kilometers and A_{max} = maximum trace amplitude in nanometers (instead of μm in a WA record). This amplitude is measured on the output from a horizontal-component seismograph that is filtered so that the response of the seismograph/filter system replicates that of a WA standard seismograph but with a static magnification of one. The underlying procedure of M_L determination according to relation (2) was adopted by the International Association of Seismology and Physics of the Earth's Interior (IASPEI) in 2004 as the standard procedure for determining local magnitudes in the distance range up to typically less than 1000 km [42]. For earthquakes in the Earth's crust of regions with attenuation properties that differ from those of coastal California, and for measuring M_L with vertical component seismographs, the standard equation takes the form:

$$M_L = \log_{10}(A_{max}) + F(R) + G \quad (3)$$

where $F(R)$ is an R-dependent calibration function and G a constant which have to compensate for different regional attenuation and/or for any systematic biases of amplitudes measured on vertical instead on horizontal seismographs. Examples of regional M_L calibration functions developed for different parts of the world have been compiled by Bormann (Chap. 3, p. 26, and DS 3.1 in [6]).

A few decades ago, analog seismic records prevailed. They had a rather limited dynamic range of only some 40 dB. This caused record traces often to go off-scale when stronger seismic events were recorded at local or regional distances. Then A_{max} could not be measured. Yet, it was found that the duration **d** of the coda that follows A_{max} with exponentially decaying amplitudes (see Fig. 1) increases with magnitude and distance D. On this basis, local duration magnitude formulas of the following general form

$$M_d = a + b \log \mathbf{d} + cD \quad (4)$$

have been developed with a, b and c being coefficients to be determined locally. When using only recordings at distances $D < 100$ km the distance term cD is not even needed. However, crustal structure, scattering and attenuation conditions vary from region to region. Moreover, the resulting specific equations will also depend on the chosen definition for **d**, the local signal-to-noise (SNR) conditions and the sensor sensitivity at the considered seismic station(s) of a network. Therefore, M_d scales have to be determined locally for a given source-network configuration and scaled to the best available amplitude-based M_L scale.

Nowadays digital recorders with large usable dynamic range of about 140 dB are common. Thus even sensitive modern broadband seismographs remain on scale when recording local or regional earthquakes up to $M \approx 7$. This reduces the need for M_d scales. Moreover, the increasing availability of modern strong-motion (SM) recorders with comparably large dynamic range, which will not clip even in the case of very strong nearby earthquakes, have led to

the development of (partially) frequency-dependent M_L^{SM} scales. They are usually based on the calculation of synthetic WA seismograph outputs from strong-motion accelerograms [35,54].

Also, amplitudes of short-period L_g waves with periods around 1 s are sometimes used to determine magnitudes, termed $m_b(L_g)$. L_g waves travel with group velocities of 3.6 to 3.2 km/s and arrive after the (secondary, shear) *S* wave onset (Fig. 1). They propagate well in continental platform areas. Recently, the IASPEI [42] adopted a measurement procedure for $m_b(L_g)$ as international standard, which had been developed for eastern North America [62] with the aim to improve yield estimates of Nevada Test Site explosions. However, as for all other local or regional magnitude scales, the calibration term is strongly influenced by the local/regional geologic-tectonic conditions in the Earth's crust and requires a proper scaling to this standard, when applied to other areas than eastern North America.

Tsuboi developed for the Japan Meteorological Agency (JMA) in 1954 [79] a magnitude formula for shallow earthquakes (depth $h < 60$ km) that have been recorded at epicentral distances D up to 2000 km:

$$M_{JMA} = \log_{10} A_{max} + 1.73 \log_{10} D - 0.83 . \qquad (5)$$

A_{max} is the largest ground motion amplitude (in μm) in the total event record of a seismograph with an eigenperiod of 5 s. If horizontal seismographs are used then $A_{max} = (A_{NS}^2 + A_{EW}^2)^{1/2}$ with A_{NS} and A_{EW} being half the maximum peak-to-trough amplitudes measured in the two horizontal components. This formula was devised to be equivalent to the medium to long-period Gutenberg–Richter [29] magnitude *M*. Therefore, M_{JMA} agrees rather well with the *seismic moment* magnitude M_w. The average difference is less than 0.1 in the magnitude range between 4.5 and 7.5 but becomes > 0.5 for $M_w > 8.5$ (see Fig. 4). Katsumata [49,50] has later modified the M_{JMA} formula for earthquakes deeper than 60 km.

Another, more long-period regional moment magnitude scale, termed M_{wp}, has been developed in Japan as well [80]. It provides quick and less saturating magnitude estimates for tsunami early warning. Velocity-proportional records are twice integrated and approximately corrected for geometrical spreading and an average *P*-wave radiation pattern (see *source mechanism*) to obtain estimates of the scalar *seismic moment* M_o at each station. Usually the first maximum in the integrated displacement trace, called "moment history" $M_o(t)$, is assumed to represent M_o. From these M_o values moment magnitudes M_w are then calculated for each station according to Eq. (11) and averaged. M_{wp} results from adding an empirically derived correction of 0.2 m.u. to the averaged station M_w [80]. Finally, a magnitude-dependent correction is applied to M_{wp} [86] in order to get an even better estimate of the recognized "authoritative" Global Centroid Moment Tensor magnitude M_w (GCMT) which is calculated according to the Harvard procedure [23] and now published under [41].

The M_{wp} concept was originally developed for earthquakes at $5° \leqslant D° \leqslant 15°$, but can be applied for $M_w < 7.5$ (down to about $M_w \approx 5$) even to shorter local distances as long as this distance is significantly larger than the rupture length. Later the M_{wp} procedure has been adopted for application to records of deep and teleseismic earthquakes as well [81]. M_{wp} estimates are standard routine in Japan, at the Alaska and the Pacific Tsunami Warning Centers (ATWC and PTWC), and the National Earthquake Information Center (NEIC) of the United States Geological Survey (USGS). However, each of these centers use slightly different procedures. Values for most strong earthquakes are usually available some 10 to 15 min after the origin time (OT). On average M_{wp} data scale well with M_w. Exceptions, however, are extremely slow or very large complex earthquakes. Then M_{wp} is usually too small, up to about 1 m.u.

In recent years great attention is paid to the development of even more rapid earthquake early warning systems (EWS). They aim at event location and magnitude estimates from the very first few seconds of broadband acceleration, velocity or displacement records and within about 10 to 30 s after origin time (OT) of strong damaging earthquakes on land. These data are to be used for instantaneous public alarms and/or automatically triggered risk mitigation actions after strong earthquakes with damage potential. The goal is to minimize the area of "blind zones" which are left without advanced warning before the arrival of the *S* waves which have usually the largest strong-motion amplitudes (see Fig. 1). This necessitates very dense and robust local seismic sensor networks within a few tens of kilometers from potentially strong earthquake sources. Such networks are at present available only in very few countries, e. g. in Japan, Taiwan, Turkey, and Italy.

Their principles of rapid magnitude estimates differ from those mentioned above and below and the data analysis from such systems is largely based on still much debated concepts such as the hypothesis of the deterministic nature of earthquake rupture [66,73]. Data presented in [66] seem to suggest that in the range $3.0 < M$ (not specified) < 8.4 the magnitude can be estimated with an average absolute deviation of 0.54 m.u. from the maximum period within the initial 4 s of the first arriving

(primary, longitudinal) *P* wave when many low-pass filtered velocity records within 100 km from the epicenter are available. However, for $M > 6$ the systematic increase of these greatly scattering periods becomes rather questionable. When analyzing waveforms of the Japanese Hinet seismic network [73], it could not be confirmed that such a dominant frequency scaling with magnitude exists. Also Kanamori [46], together with Nakamura [60,61], one of the fathers of this idea, expressed much more caution about the prospects of this method after he had run, together with Wu [89], an experiment with the Taiwan EWS. For each event they analyzed the first 3 s of at least eight *P*-wave records at epicentral distances < 30 km. They knew that: "… the slip motion is in general complex and even a large event often begins with a small short-period motion, followed by a long-period motion. Consequently, it is important to define the average period during the first motion." (termed τ_c in [46,89]). However, after applying the τ_c concept to the Taiwan EWS they concluded: "For EWS applications, if $\tau_c < 1$ s, the event has already ended or is not likely to grow beyond $M > 6$. If $\tau_c > 1$ s, it is likely to grow, but how large it will eventually become, cannot be determined. In this sense, the method provides a threshold warning". Thus it seems that these new concepts work reasonably well only for earthquakes with $M < 6.5$ and thus total rupture durations that are according to Eq. (13) on average not more than about 2–3 times the measurement time windows of 3 s or 4 s used in [46,66,89]. Nakamura and Saita [61] reported data from a much smaller set of events ($N = 26$) recorded at local distances in the range $4.6 < M < 6.9$. We calculated the average absolute deviation of their rapid UrEDAS system magnitudes (0.47 m.u.) from the official magnitudes M_{JMA} published later by the Japan Meteorological Agency. This error decreases to 0.32 m.u. when only earthquakes with magnitudes up to $M_{JMA} = 6.0$ are considered. This seems to support our assessment that the reliability of real-time EMS magnitudes decreases rapidly if the analyzed time window is much shorter than the rupture duration.

Magnitude Scales Used in the Teleseismic Distance Range ($D > 2000$ km)

Ten years after the introduction of the local magnitude M_L, Beno Gutenberg [26,27,28] extended the concept of magnitude determination to teleseismic distances larger than about 1000–2000 km. He used both records of seismic waves that propagate along the Earth's surface (or near to it with a period-dependent penetration depth) and waves which travel through the Earth. Accordingly, the former are termed surface waves and the latter body waves. For the surface-wave magnitude Gutenberg [28] gave the following relation:

$$M_S = \log_{10} A_{Hmax} + 1.656 \log D^\circ + 1.818 \qquad (6)$$

with A_{Hmax} = maximum "total" horizontal displacement amplitude of surface-waves in μm for periods around 20 ± 2 s measured in the distance range $15^\circ < D^\circ < 130^\circ$ ($1^\circ = 111{,}195$ km).

While the original Richter M_L and Gutenberg M_S magnitudes were calculated from the maximum ground displacement amplitudes, Gutenberg [26,27,30] proposed to determine the body-wave magnitudes m_B from the relation:

$$m_B = \log_{10} (A/T)_{max} + Q(D^\circ, h)\,, \qquad (7)$$

i. e., by measuring the maximum ratio of ground displacement amplitude A (in μm) divided by the related period *T* (in s). A/T is equivalent to measuring the maximum ground motion velocity $A_{vmax}/2\pi$ which is proportional to the square root of *seismic energy*, i. e. $\sqrt{E_s}$. Thus the magnitude becomes a measure of the elastic kinetic wave energy radiated by an earthquake. Only in this way comparable magnitude data could be obtained for different types of body waves and measurements at different sites. Another great advantage of m_B is that it permits magnitude estimates also from intermediate and deep *earthquake sources*, which produce only weak or no surface waves at all. Empirical relationships permit estimating E_s (in units of Joule) from body-wave magnitude m_B [30]

$$\log_{10} E_s = 2.4\, m_B - 1.2 \qquad (8)$$

or surface-wave magnitude M_S [72]

$$\log_{10} E_s = 1.5\, M_S + 4.8\,. \qquad (9)$$

Accordingly, an increase by 1 m.u. in m_B and M_S corresponds to an increase of radiated seismic energy by about 250 and 30 times, respectively.

Revised empirical distance-depth corrections for the calibration of body-wave magnitudes, so-called *Q*-functions, were published in 1956 by Gutenberg and Richter [30]. They are given as separate tables and charts for the body-wave phases *P*, *PP* (a *P* wave reflected at the surface of the Earth about the half way between source and station) and *S*. They are still in use, especially Q_{PV} for calibrating amplitude measurements made on vertical component *P*-wave records (Fig. 2). However, for epicenter distances between 5° and 20° these calibration values are not reliable enough for global application. In this range

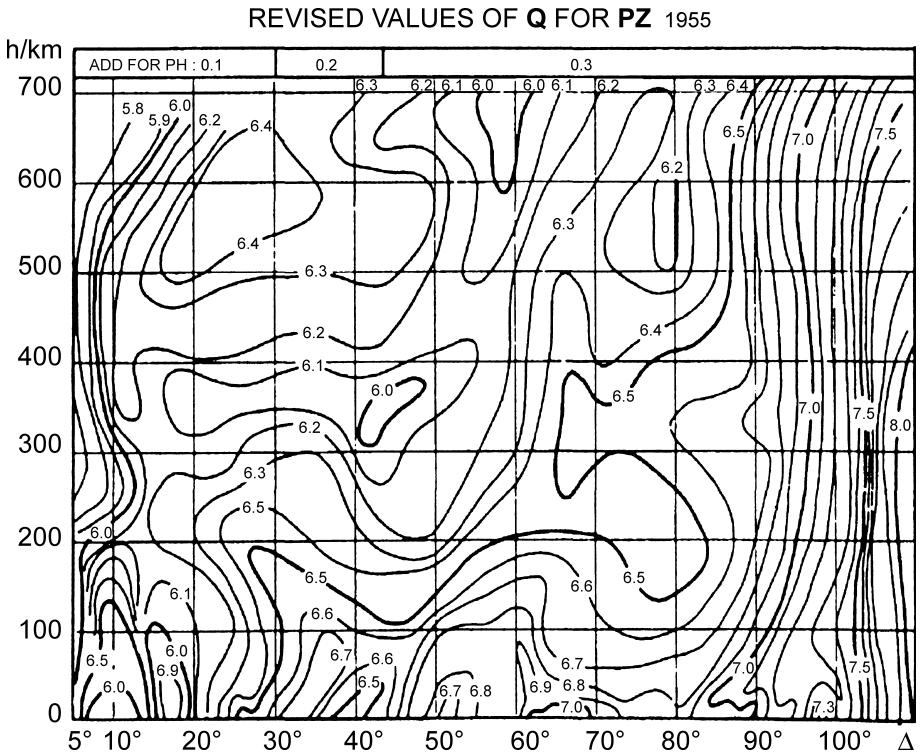

Earthquake Magnitude, Figure 2
Calibration values $Q(D^\circ, h)$ for vertical (Z) component P-wave amplitudes depending on epicentral distance $D^\circ = \Delta$ and source depth h as used in the calculation of body-wave magnitudes m_b and m_B according to Gutenberg and Richter, 1956 [30]

the wave propagation is strongly affected by regional variations of the structure and properties of the Earth's crust and upper mantle. And for $D > 100°$ the P-wave amplitudes decay rapidly because of the propagation of P waves is influenced by the Earth's core (so-called core shadow). Therefore, in agreement with current IASPEI recommendations [42], m_B and its short-period complement m_b (see below), should be determined by using Q_{PV} only between $21° \leqslant D \leqslant 100°$.

These body-wave magnitude calibration functions had been derived from amplitude measurements made mostly on medium-period broadband displacement records which dominated during the first half of the 20th Century at seismological stations. Their period-dependent magnification curve resembled more or less that of the classical standard seismograph type C shown in Fig. 3, although for some of these instruments the roll-off of the amplification occurred already at periods $T > 10$ s.

Another, so-called Prague–Moscow formula for surface-wave magnitudes was proposed in 1962 by Vaněk et al. [84]. It is based on the measurement of $(A/T)_{max}$ in records of shallow earthquakes ($h < 60$ km) in wide period and distance ranges ($3\,\text{s} < T < 30\,\text{s}$; $2° \leqslant D° \leqslant 160°$):

$$M_S = \log_{10}(A/T)_{max} + 1.66 \log_{10} D^\circ + 3.3\,. \qquad (10)$$

This relationship, which is – as Eq. (7) – more directly related to E_s, was adopted by the IASPEI in 1967 as international standard.

The NEIC adopted Eq. (10), but continues to limit the range of application to distances between $20° \leqslant D° \leqslant 160°$ and displacement amplitudes in the very limited period range as in formula (6) although Soloviev [74] had shown already in 1955 that $(A/T)_{max}$ is a stable quantitative feature of surface waves whatever the period of their maximum at all epicentral distances. Also theory has confirmed [63] that using the ratio (A/T) is a partial and ad hoc compensation for a large number of frequency-dependent terms ignored in (10). In fact, the periods at the surface-wave maximum used for M_S determination vary in a wide range between some 3 s and 25 s and show – despite large scatter – a clear distance dependence [84,87]. Therefore, several authors [36,70] showed that using Eq. (10) only for amplitude readings around 20 s results in system-

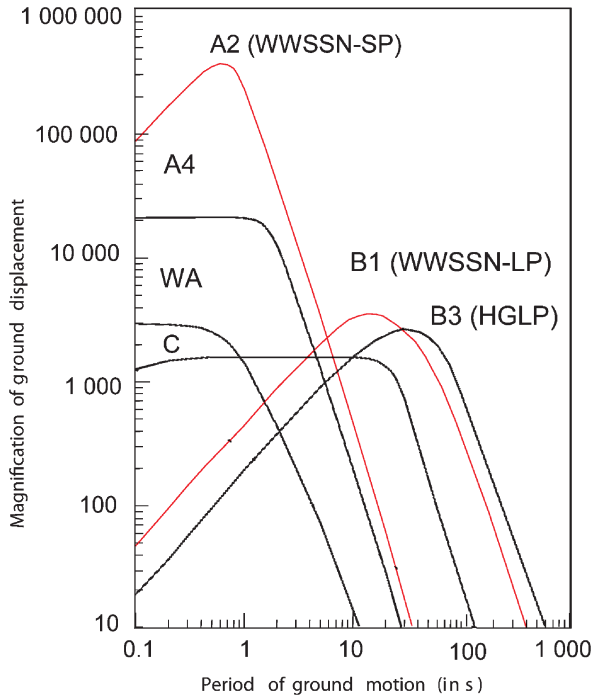

Earthquake Magnitude, Figure 3
Magnification of ground displacement amplitudes by common standard types of seismographs. WA = Wood–Anderson seismograph; WWSSN-SP and WWSSN-LP = short-period and long-period seismographs used in the former United States World-Wide Seismograph Standard Network; HGLP = US type of High Gain Long Period seismographs; A2, A3, B1, B3 and C = standard types of seismographs according to Willmore [87]. Reprint from [6] with © granted by IASPEI

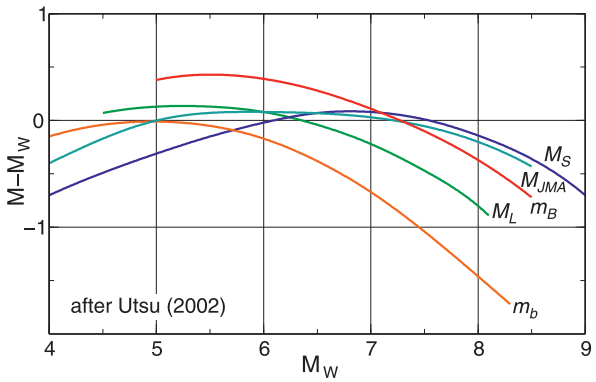

Earthquake Magnitude, Figure 4
Average relationships between different common types of magnitudes and the moment magnitude M_w. Modified from Fig. 1 in [83]

atic distance-dependent biases. However, their proposed revised calibration functions for 20 s waves are not yet used in routine practice at international seismological data centers.

The formulas (6) and (10) had originally been developed for horizontal component amplitude readings. Beginning in the 1960s, however, more and more long-period and broadband vertical component instruments became available and are now commonly used for magnitude determination from surface waves. This procedure is easier and better defined than measuring and combining the amplitude measurements made in two horizontal components, yields on average values that are largely comparable with the Gutenberg M_S [25] and has recently been adopted as IASPEI [42] standard. Herak et al. [37] published theoretical and observed depth corrections for $M_S(20)$ when determined according to (10). These corrections allow determination of more reliable surface-wave magnitudes for earthquakes in all depth ranges and improve significantly the relationship between M_S and the *seismic moment* M_o.

In the 1960s, the United States deployed a World-Wide Standard Seismograph Network (WWSSN) equipped with short-period (SP) and long-period (LP) seismographs of limited bandwidth (cf. Fig. 3). This network had two priority tasks. Firstly, to significantly increase the signal-to-noise ratio of the seismic records by narrow-band short-period filtering, thus improving the global detection threshold for teleseismic events down to magnitudes around 4–4.5 and the location accuracy for seismic events. Secondly, to realize an effective discriminator between underground nuclear explosions (UNE) and natural earthquakes based on the ratio of a short-period body-wave and a long-period surface-wave magnitude. Natural earthquakes have a much longer source duration (seconds to minutes) than explosions of comparable size (typically milliseconds). Also, at comparable *seismic moment* magnitude, UNEs radiate significantly more high-frequency energy (see dotted curve in Fig. 5) than earthquakes. Therefore, a better discrimination of the two types of events was achieved by measuring the *P*-wave amplitude only at periods < 3 s (typically around 1 s) and calculating a short-period *P*-wave magnitude termed m_b. In contrast, the Gutenberg m_B is based on measuring A_{max} at periods T usually between 2 s and 30 s. Further, during the first two decades of the WWSSN, the *P*-wave amplitude was not – as required by Gutenberg's procedure for m_B determination – always measured at the maximum of the whole *P*-wave train (whose length depends on the source duration and thus on the magnitude itself) but initially within the first five half-cycles only and later by USGS requirement in the first 5 s of the record.

Because of the short source duration of explosions, their *P*-waves will always reach maximum amplitudes

within such a short time-interval. However, *P* waves radiated by large earthquakes of much longer source duration will reach their maximum amplitude usually much later in the rupture process. For magnitude 6 the average rupture duration is on average already 6 s, and may increase to about 600 s for the strongest earthquakes (cf. relation (13)). Both effects together, plus the fact, that m_b was still computed using the Q_{PV} function derived for mainly medium-period *P* waves, which are much less affected by frequency-dependent attenuation than 1 Hz *P* waves, resulted in a systematic underestimation of the earthquake size for magnitudes larger than 5 and a *saturation* of m_b at around 6.5.

In the late 1970s, the NEIC switched back to a longer time window of about 15 s and more recently, with an automatic procedure, to a window covering the first 10 cycles of short-period teleseismic *P* waves. In the case of strong earthquakes this window may later be extended interactively up to 60 s. This mitigates to some extend the saturation of m_b. However, no m_b-values larger than 7.2 have ever been measured with this procedure. On the other hand m_b yields rather reliable values for magnitudes < 5 when the corner frequency of the average source spectra falls within the passband of the short-period seismograph or is even more high frequency (cf. Figs. 3, 4, 5). For magnitudes < 5 m_B can usually no longer be determined because of too small signal-to-noise ratio (SNR) in broadband records. Then m_b is often the only available teleseismic estimator of earthquake size for small earthquakes.

Most seismic stations and networks worldwide adopted the US procedure for m_b measurement and – with the exception of Russia, China and their former allies – completely abandoned measuring m_B as originally defined. This change in attitude was stimulated by the fact that the NEIC, which serves in fact as one of the leading international data centers for seismology, did not accept reported *P*-wave amplitudes other than those obtained from short-period measurements. Some stations, national and global data centers continue (at least up to 2008) to measure for m_b the maximum amplitude of *P* exclusively within the first 5 s after the *P*-wave *first arrival*, such as the China Earthquake Network Center and the International Data Center (IDC) of the Comprehensive Test-Ban Treaty Organization (CTBTO) in Vienna.

Because of these inconsistencies in m_b and M_S determination and the proven merits of both broadband m_B and M_S (see also [11]) the IASPEI Working Group on Magnitude Measurements recommended that in future:

a) m_b is always determined from A_{max} at periods $T < 3$ s within the whole *P*-wave train;

b) The band-limited magnitudes m_b and $M_S(20)$ be complemented by true broadband magnitudes m_B and M_S(BB). The latter two will be obtained by measuring A_{vmax} on unfiltered velocity broadband records and thus always include the maximum velocity amplitudes of the source spectrum in the magnitude range of interest (cf. Fig. 5). This will link these two broadband magnitudes to the seismic energy released by an earthquake, more closely than the common band-limited magnitudes.

These recommendations have been adopted by the IASPEI Commission on Seismic Observation and Interpretation (CoSOI) in 2005 as new magnitude measurement standards. More details about the new measurement procedures for m_b, m_B, $M_S(20)$ and M_S(BB) are given on the CoSOI web site [42]. Beginning in 2007 they are gradually implemented at the main seismological data centers and networks.

Since all magnitudes discussed so far show more or less pronounced *saturation* for large earthquakes (cf. Fig. 4 and [44]) a non-saturating magnitude, termed M_w, has been proposed [31,43,69]. The moment magnitude M_w is derived from the scalar *seismic moment* M_o via the relation

$$M_w = (2/3)(\log_{10} M_o - 9.1)\,. \tag{11}$$

M_o has the dimension of Newton meter (Nm) and expresses the total inelastic "work" required for rupturing and displacing the considered earthquake fault. It can be determined either by waveform analysis and inversion in the time domain or by measuring the spectral amplitude $u_{0p,s}$ of the low-frequency level (plateau) of the displacement spectrum of *P* or *S* waves (cf. Fig. 5) via the relationship

$$M_o = 4\pi r \rho\, v_{p,s}^3 u_{0p,s} / R_{\theta,\phi}^{p,s} \tag{12}$$

with r = hypocenter distance, ρ = average density of rocks in the source and receiver area, $v_{p,s}$ = average velocity of the *P* or *S* waves from the source to the receiver area and $R_{\theta,\phi}^{p,s}$ = a factor correcting the observed seismic amplitudes for the influence of the radiation pattern of the given *source mechanism*, which is different for *P* and *S* waves.

M_o is expected to show no *saturation*, provided that the amplitude level is measured only at periods significantly larger than the magnitude-dependent *corner period* of the seismic source spectrum (cf. Fig. 5). In Sects. "Common Magnitude Estimates for the Sumatra 2004 M_w 9.3 Earthquake" and "Magnitude Saturation and Biases Due to Earthquake Complexity" we will show, however, that in-

correct determination of M_o may still result in an underestimation of the earthquake size. Since M_w is derived from M_o it is related to the tectonic effect of earthquakes, i. e., to the product of rupture area and average fault slip and thus also relevant to assess the tsunami potential of strong shallow marine earthquakes. An example is the off-shore Nicaragua earthquake of 2 September 1992. Its $m_b = 5.3$ was too weak to alert the people ashore, some 70–120 km away from the source area. However, its $M_w = 7.6$ was much larger and caused a damaging local tsunami with almost 200 casualties.

Yet, M_o and thus M_w do not carry any direct information about the dominant frequency content and thus of the seismic energy released by the earthquake (cf. Sect. "Magnitude Saturation and Biases Due to Earthquake Complexity"). In fact, relation (11) was derived by assuming constant stress drop and an average ratio of $E_s/M_o = 5 \times 10^{-5}$ on the basis of elastostatic considerations and empirical data [43] and then replacing in Eq. (9) M_S by M_w.

As source theory has advanced and broadband digital data have became readily available, the radiated *seismic energy* E_s could be computed explicitly rather than from an empirical formula. Boatwright and Choy (cf. [5,16]) developed such an algorithm for computing E_s as well as a related energy magnitude M_e which agrees with M_w for $E_s/M_o = 2 \times 10^{-5}$. E_s is computed by integrating squared velocity-proportional broadband records over the duration of the *P*-wave train, corrected for effects of geometrical spreading, frequency-dependent attenuation during wave propagation and source radiation pattern. According to [16], the radiated seismic energy may vary for a given seismic moment by two to three orders of magnitude. Further, it was found that a list of the largest events is dominated by earthquakes with thrust mechanisms when size is ranked by moment, but dominated by strike-slip earthquakes when ranked by radiated seismic energy. Choy and Kirby [18] gave a striking example for differences between M_e and M_w for two Chile earthquakes in 1997 which occurred in the same area but with different *source mechanisms*. One was interplate-thrust with $M_w = 6.9$ and relatively low $M_e = 6.1$, whereas the other was intraslab-normal with $M_w = 7.1$ and rather large $M_e = 7.6$. The first earthquake had a low potential to cause shaking damage and was felt only weakly in a few towns. In contrast, the second one caused widespread damage, land- and rockslides, killed 300 people and injured 5000. Thus, M_w, although it theoretically does not saturate, may strongly underestimate or overestimate the size of an earthquake in terms of its potential to cause damage and casualties. Shaking damage is mainly controlled by the relative amount of released high-frequency energy at $f > 0.1$ Hz which is better measured by M_e.

The quantity $\tau_a = \mu E_s/M_o$ is termed apparent stress [90]. It represents the dynamic component of stress acting on the fault during slip, which is responsible for the generation of radiated kinetic seismic wave energy E_s. On average it holds that $\tau_a \approx 2\Delta\sigma$ (with $\Delta\sigma$ = stress drop = difference between the stress in the source area before and after the earthquake rupture). Both τ_a and $\Delta\sigma$ depend strongly on the seismotectonic environment, i. e., the geologic-tectonic conditions, fault maturity and type of earthquake *source mechanisms* prevailing in seismically active regions [16,17,18,19]. However, $M_e \approx M_w$ holds only for $\tau_a \approx 0.6$ MPa.

Another important teleseismic magnitude is called mantle magnitude M_m. It uses surface waves with periods between about 60 s and 410 s that penetrate into the Earth's mantle. The concept has been introduced by Brune and Engen [13] and further developed by Okal and Talandier [64,65]. M_m is firmly related to the seismic moment M_o. Best results are achieved for $M_w > 6$ at distances > 15–$20°$ although the M_m procedure has been tested down to distances of 1.5° [77]. However, at $D < 3°$ the seismic sensors may be saturated in the case of big events. Also, at short distances one may not record the very long periods required for unsaturated magnitude estimates of very strong earthquakes, and for $M_w < 6$, the records may become too noisy at very long-periods. A signal-to-noise ratio larger than 3 is recommended for reliable magnitude estimates. M_m determinations have been automated at the PTWC and the CPPT [39,85] so that estimates are available in near real-time within about 10 min after OT from near stations, however typically within about half an hour, plus another few minutes for great earthquakes measured at the longest periods. Since M_m is determined at variable very long periods this magnitude does not – or only marginally – saturate even for very great, slow or complex earthquakes.

Common Magnitude Estimates for the Sumatra 2004 M_w 9.3 Earthquake

On 26 December 2004, the great Sumatra–Andaman Island earthquake with a rupture length of more than 1000 km occurred. It caused extensive damage in Northern Sumatra due to strong earthquake shaking. Moreover, it generated an Indian Ocean-wide tsunami with maximum run-up heights of more than 10 m. In total, this event claimed more than 200,000 victims and caused widespread damage on the shores of Sumatra, Thailand, India and Sri Lanka that were reached by the tsunami wave

within some 15 min to about two hour's time. This earthquake put the current procedures for magnitude determination to a hard test both in terms of the reliability and compatibility of calculated values and the timeliness of their availability to guide early warning and disaster management activities. Here we address only seismological aspects, not the additional major problems of inadequate global monitoring and insufficient regional communication and disaster response infrastructure. The earliest magnitudes reported by or made available to the Pacific Tsunami Warning Center (PTWC) were:

- $m_b > 7$, about 8 min after origin time (OT);
- $M_{wp} = 8.0$, available after some 12 minutes at the PTWC (including a magnitude-dependent correction [86]);
- somewhat later in Japan $M_{wp} = 8.2$ after magnitude-dependent correction [48];
- $M_m \geqslant 8.5$ at the PTWC about 45 min after OT, hours later upgraded to $M_m = 8.9$ by using mantle surface waves with longer periods ($T \approx 410$ s);
- a first surface-wave magnitude estimate $M_S = 8.5$, some 65 min after OT;
- $M_w = 8.9$ (later revised to 9.0) released by Harvard Seismology more than 6 h after OT.

Other available measurements were: $m_b = 5.7$ and $M_S = 8.3$ by the IDC of the CTBTO, $m_b = 7.0$, $M_S = 8.8$, $M_e = 8.5$ and another long-period *P*-wave based $M_w = 8.2$ by the NEIC. All these values were too small and mostly available only after several hours or days (e. g., IDC data). Weeks later, after the analysis of Earth's *fundamental modes* with periods up to 54 min and wavelength of several 1000 km, the now generally accepted value $M_w = 9.3$ was published [76]. Why were the other magnitude values all too low and/or too late?:

- m_b NEIC suffers from the combined effect of both spectral and time-window dependent saturation that we will discuss in more detail in Sect. "Magnitude Saturation and Biases Due to Earthquake Complexity";
- m_b IDC is even more affected by these saturation effects, because of the very short measurement time window of only 5 s after the first *P*-wave onset. In the case of the Sumatra 2004 earthquake, the first *P*-wave maximum occurred after some 80 s and another, with comparable amplitude, after about 330 s (cf. Fig. 8). Further, prior to m_b measurement, the IDC broadband data are filtered with a more narrow-band response peaked at even higher frequencies (3–4 Hz) than at NEIC ($\approx$ 2.5 Hz) [11];
- The reported surface-wave magnitudes ranged between $M_S = 8.3$ (IDC), 8.8 (NEIC and Japan Meteorological Agency) and 8.9 (Beijing), i. e., some of them are close to the moment magnitudes. However, because of the late arrival of long-period teleseismic surface waves, good estimates are usually not available within 1–2 h after OT. This leaves a sufficient tsunami warning lead time only for shores more than 1000–2000 km away from the source.
- The NEIC *P*-wave moment magnitude $M_w = 8.2$ was to small because its procedure is, similar as for M_{wp} determinations, based on relatively short-period (typically $T < 25$ s) *P*-wave recordings and a single-source model (cf. Sect. "Magnitude Saturation and Biases Due to Earthquake Complexity").
- The preliminary $M_e = 8.5$, computed a few hours after the December 2004 earthquake agreed with the final M_e computed later using a more robust method [20]. Another algorithm simulating a near-real-time computation would have yielded $M_e = 8.3$. Yet M_e, by its very nature as an energy magnitude and because of the relation $E_s = \Delta\sigma/2\mu\, M_e$, will generally be smaller than M_w for slow, long duration earthquakes with low stress drop. This is often the case for shallow thrust earthquakes in subduction zones. Extreme examples are four well-known slow tsunami earthquakes of 1992 (Nicaragua; $M_w = 7.6$, $\Delta M_e = -0.9$), 1994 (Java; $M_w = 7.8$, $\Delta M_e = -1.3$), 2000 (New Britain Region; $\Delta M_w = 7.8$, $\Delta M_e = -1.0$) and 2006 (Java; $M_w = 7.7$, $\Delta M_e = -0.9$) [40].

Magnitude Saturation and Biases Due to Earthquake Complexity

Currently, the most common magnitude scales, especially those based on band-limited short-period data, still suffer *saturation*, e. g., the magnitudes m_b, M_L, m_B and M_S, which are typically measured at periods around 1 s, 2 s, 5–15 s and 20 s, respectively begin to saturate for moment magnitudes M_w larger than about 5.5, 6.5, 7.5 and 8.0. Earthquakes with $m_b > 6.5$, $M_L > 7.0$, $m_B > 8.0$ and $M_S > 8.5$ are rare been found due to saturation (cf. Fig. 4 and [44]). Magnitude saturation has two causes: spectral saturation and saturation due to insufficient time-window length for the amplitude measurements. Source complexity may cause additional biases between different magnitude scales.

Spectral Saturation of Magnitudes

Spectral saturation occurs when the magnitude-dependent *corner frequency* f_c (for energy-related magnitudes) or

the low-frequency plateau of displacement amplitudes (for moment magnitude) fall outside of the passband range of the seismographs *transfer function* or magnification curve (Fig. 3) of the recording seismograph or of the filter applied to broadband data before magnitude measurements are made. The reason for spectral saturation can best be explained by way of idealized average "source spectra" of ground displacement $u(f)$ and ground velocity $v(f)$ that have been corrected for the instrument response, for the decay of the wave amplitudes due to attenuation that is caused by internal friction and scattering of the seismic waves at heterogeneities of the Earth and for amplification effects at the surface of the receiver site. For better understanding such source spectra have been multiplied in Fig. 5 by the factor $4\pi r\rho\, v_{\mathrm{p,s}}^3/R_{\theta,\phi}^{p,s}$ given in Eq. (12) in order to get for the displacement amplitudes $u_0 =$ constant at $f < f_\mathrm{c}$ the related scalar seismic moment M_o (Fig. 5, left) and its time-derivative, the so-called moment rate (Fig. 5, right).

The shape of the source spectrum can be interpreted as follows: The critical wavelength, which corresponds to f_c, is $\lambda_\mathrm{c} = v_{\mathrm{p,s}}/f_\mathrm{c} = c_{\mathrm{m1}}\pi R = c_{\mathrm{m2}}\,(\mathrm{L}\times\mathrm{W})^{1/2}$ with $v_{p,s}$ – velocity of the *P* or *S* waves in the source region, depending on whether f_c relates to a *P*-wave or an *S*-wave spectrum, *R*-radius of a circular fault rupture model, L– length and W– width of a rectangular fault rupture model; c_{m1} and c_{m2} are model dependent constants. For very long fault ruptures, i. e., $L \gg W$, one can even write $\lambda_\mathrm{c} = c_{\mathrm{m3}}L$. Thus, λ_c is proportional to the linear dimension of the fault. For $f < f_\mathrm{c}$, λ_c becomes larger than the fault. Rupture details along the fault can then no longer be resolved and the fault is "seen" by these long wavelengths just as a point source. Therefore, all frequencies $f < f_\mathrm{c}$ have the same displacement amplitudes. Accordingly, M_o, which is proportional to the fault area and the average slip over the fault, has to be determined either in the spectral domain from the low-frequency asymptote u_o to the displacement spectrum or in the time domain by fitting synthetic long-period waves with $f < f_\mathrm{c}$ to observed ones that have been low-pass filtered in the same frequency range.

For radiated frequencies $f > f_\mathrm{c}$ with $\lambda < \lambda_\mathrm{c}$, the shape of the spectrum changes drastically. Related displacement amplitudes are then excited by successively smaller patches of the rupture plane. The area of the rupture elements decreases with the second order of their linear dimension. Accordingly, the generated displacement amplitudes are $A_\mathrm{d} \sim f^{-2}$, while the related velocity amplitudes $A_\mathrm{v} = A_\mathrm{d} 2\pi f$ decay only $\sim f^{-1}$. In the seismological literature this is usually called the ω^{-2} rupture model [3], based on the concept of similarity, which implies a constant stress drop independent of source size. More complicated rupture models yield a high-frequency amplitude decay $\sim \omega^{-3}$ [33,34] and even more rapid decays have sometimes been found in empirical data (up to 5th order). Steeper than ω^{-2} amplitude decay would further amplify the spectral saturation of magnitude data discussed below.

The Harvard standard procedure for M_o determination assumes a single point source model with a prescribed, triangular moment-rate function in the time domain (as an approximation to moment-rate curves such the ones shown in Fig. 7) as well a minimum period of 200 s for strong earthquakes with magnitudes > 8. Assuming an average rupture velocity of 2.5 km/s, this period would correspond to a wavelength of 500 km. This is much shorter than the total rupture length of more than 1100 km for the great Sumatra 2004 earthquake and explains why $M_\mathrm{w}(\mathrm{HRV}) = 9.0$ was smaller than the moment magnitude $M_\mathrm{w} = 9.3$ determined by using fundamental Earth's modes with periods of 1000 s and more [76].

The relationship between the two currently most common magnitudes, m_b and $M_\mathrm{S}(20)$, can be understood with reference to Fig. 5. m_b is measured in the period range $0.5 < T < 3$ s, typically around 1 s. This corresponds approximately to the *corner frequencies* of earthquakes with $M_\mathrm{S} \approx 3$ to 4.5. According to Utsu [83] this is equivalent to an m_b between about 3.5 and 5.0. For $M_\mathrm{S} < 4.5$ or $m_\mathrm{b} < 5$, m_b is thus likely to be determined from amplitude measurements near or below the *corner frequency* of the source spectrum. In that case m_b is a good measure of seismic moment. However, for larger magnitudes m_b samples spectral amplitudes well above f_c, resulting in systematically too small m_b values as compared to M_S and M_w. For great earthquakes this difference may reach 2 m.u. (Fig. 4). In contrast, $M_\mathrm{S}(20)$ is measured at periods around 20 s and thus saturates much later at values between about 8.5 to 9.

However, these arguments only hold on average. The stress drop $\Delta\sigma$ of individual events may vary by about 2 to 3 orders, as apparent stress τ_a, especially for earthquakes with $M_\mathrm{w} < 7.5$ [16,17]. According to the relation $M_\mathrm{o} = (16/7)\Delta\sigma R^3$ given by Keilis–Borok [52] this may change source radii R and associated f_c by about one order. As an example, the dotted curve in Fig. 5 shows the approximate seismic source spectrum for a well contained underground nuclear explosion (UNE) of an equivalent yield of 1 kt TNT which corresponds to a magnitude $m_\mathrm{b} \approx 4$. Its source volume is much smaller than that of an earthquake with same seismic moment. Hence the *corner frequency* of its source spectrum is not around 1 Hz but around 10 Hz. This is the reason why m_b determined from UNE records does not saturate, even for the strongest UNE ever tested with $m_\mathrm{b} \approx 7$. Moreover, Fig. 5 also illustrates that an earthquake and an UNE

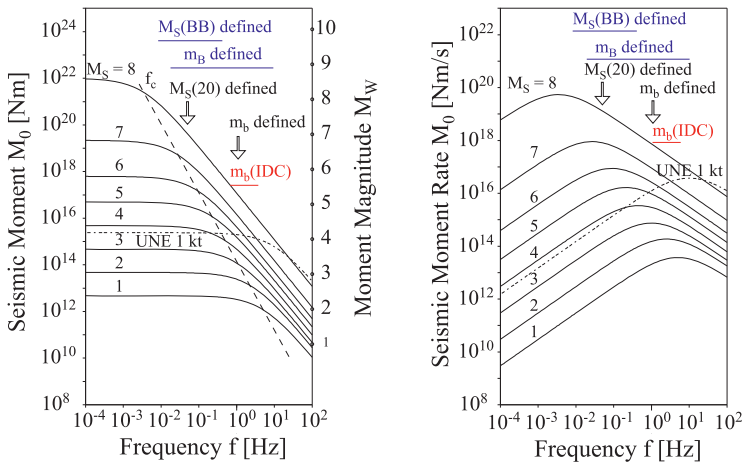

Earthquake Magnitude, Figure 5

"Source spectra" of ground displacement (*left*) and velocity (*right*) for an average single rupture seismic shear source, scaled on the left ordinates to *seismic moment* M_o (*left diagram*) and moment rate (*right diagram*), respectively. The black spectral lines have been scaled according to Aki [3] to integer surface-wave magnitudes M_S between 1 and 8. For reference the respective integer moment magnitude values M_w between 1 and 10, calculated according to Eq. (11), have been marked with equidistant dots on the right-side ordinate of the *left diagram*. The broken line shows the increase of the *corner frequency* f_c with decreasing seismic moment of the event, the dotted curve gives the approximate "source spectrum" for a well contained underground nuclear explosion (UNE) of an equivalent yield of 1 kt TNT. Note the plateau in the displacement spectrum towards low frequencies (corresponding to u_o = constant for $f < f_c$), from which M_o is determined according to Eq. (11) when using the frequency-domain approach. For $f > f_c$ the amplitudes decay $\sim f^{-2}$. The open arrows point to the center frequencies on the abscissa at which the 1Hz body-wave magnitude m_b and the 20 s surface-wave magnitude M_s(20), respectively, are determined and the blue horizontal interval bars mark the range of frequencies within which the maximum P-wave and Rayleigh-wave amplitudes for m_b and M_s(BB) should be measured according to the new IASPEI standards [37]. In contrast, the red bar marks the frequency range of maximum velocity-proportional magnification of the bandpass filter between 1 Hz and 4 Hz which is used for m_b determination at the IDC.

with seismic moment around 4×10^{15} Nm and $M_w \approx 4$ have different maximum seismic moment-rate release at about 4×10^{15} and 4×10^{16} Nm/s, respectively. The latter corresponds to 100 times higher seismic energy release or to an energy magnitude M_e that is 1.3 m.u. larger. Large differences have also been observed amongst earthquakes, e. g., the Balleny Island earthquake of 25.03.1998 had M_w(HRV) = 8.1 and M_e(NEIC) = 8.8. The opposite will happen in the case of low stress drop earthquakes propagating with very low rupture velocity [38]. The Java tsunami earthquake of 17 July 2006 was a striking example with $M_e = 6.8$, $m_B = 7.0$ and $M_w = 7.7$.

Similar observations had already been made in the 1970s when comparing m_b and M_S values of identical events. This prompted the Russian scientist Prozorov to propose a "creepex" parameter $c = M_S - a \times m_b$ (with a = constant to be determined empirically for different source types and stress drop conditions). It aims at discriminating between normal, very slow (creeping) and explosion-like (fast rupture, high stress drop) earthquakes. World-wide determination of this parameter for earthquakes in different regions revealed interesting relations of c to source-geometry and tectonic origin [51]. Similar systematic regional differences were also reported for $M_S - M_w$ [24,67] and $M_e - M_w$ [16,19], suggesting systematic regional differences in stress drop.

Magnitude Saturation Due to Insufficient Time-Window Length for Amplitude Measurement

The second reason for magnitude saturation is insufficient time-window length for measuring $(A/T)_{max}$ in seismic records. It is most relevant when determining body-wave magnitudes, but it has been a subject of controversy, misconceptions and disregard of earlier recommendations for decades. The reason is that in teleseismic seismograms the *P*-wave group does not always appear sufficiently well separated in time from later phase arrivals such as the depth phases *pP* and *sP*. These do not directly travel from the seismic source at depth h to the recording station but travel first to the Earth's surface above the source and from there, after reflection or conversion from *S* to *P*, propagate back into the Earth. Depending on h, which may vary from a few kilometers up to 700 km, and the type of depth phase recorded, they may arrive from a few seconds up to about 4.5 min after the onset of direct *P*. Depending on the radi-

ation pattern of the *source mechanism*, some stations may even record the depth phases with larger amplitudes than the direct *P* wave. This is one of the concerns that led many researchers to propose measuring the *P*-wave amplitudes for magnitude measurements within a short time window after the *P* onset. On average, however, the depth phases have smaller amplitudes than *P* and will not bias m_b estimates at all. If, however, a seismic station is situated near to the nodal line of the so-called focal sphere, corresponding to strongly reduced *P*-wave radiation in these directions, the amplitude of the depth phase is a better estimator for the body-wave energy radiated by this seismic source and thus of its corresponding magnitude.

Two or three more phases of longitudinal waves may arrive close to the direct *P* at teleseismic distances between 20° and 100°. These include *PcP*, which results from *P*-wave energy reflected back from the surface of the Earth's core at 2900 km depth, and the phases *PP* and *PPP*, which are *P* waves that have been reflected back from the Earth's surface once at half-way or twice at 1/3- and 2/3-way between the seismic source and the recording station, respectively. However, in short-period records the amplitudes of *PP* and *PPP* are generally smaller and those of *PcP* even much smaller than the amplitudes of direct *P* waves. These later arrivals will therefore, never bias m_b estimates. Yet on broadband records *PP* may sometimes have equal or even slightly larger amplitudes than primary *P*. However, *P* and *PP* phases are usually well separated by more than 1 min (up to 4 min) and not likely misinterpreted. Only for rare large earthquakes with $M > 7.5$ the rupture duration and related *P*-wave radiation may extend into the time window where *PP* should arrive. But even then, wrongly taking PP_{max} for P_{max}, the bias in m_B estimate will not exceed 0.2 m.u. and usually be much smaller.

This experience from extensive seismogram analysis practice led Bormann and Khalturin [7] to state in 1974:

> … "*that the extension of the time interval for the measurement of* $(A/T)_{max}$ up to 15 or 25 sec., as proposed …in the Report of the first meeting of the IASPEI Commission on Practice (1972) … is not sufficient in all practical cases, especially not for the strongest earthquakes with $M > 7.5$ …".

This was taken into account in the Manual of Seismological Observatory Practice edited by Willmore [87]. It includes the recommendation to extend the measurement time window for *P*-wave magnitudes up to 60 s for very large earthquakes. But still, this has not yet become common practice (see Sect. "Introduction to Common Magnitude Scales: Potential and Limitations") although even a limit of 60 s may not be sufficient for extreme events such as the Sumatra M_w 9.3 earthquake when the first $P1_{max}$ appeared around 80 s and a second $P2_{max}$ of comparable amplitude at about 330 s after the first *P*-wave onset (cf. Fig. 8).

To allow a quick rough estimate of earthquake rupture duration τ_d as a function of magnitude we derived from extrapolation of data published in [66] the average relation

$$\log \tau_d \approx 0.6M - 2.8 \,. \tag{13}$$

It yields for $M = 6, 7, 8$ and 9 $\tau_d \approx 6\,s, 25\,s, 100\,s$ and 400 s, respectively. Measurement time windows of 5 s, 25 s or 60 s may therefore underestimate the magnitude of earthquakes with $M_w > 6, > 7$ or > 8, respectively. We call this effect the time-window component of magnitude saturation. It aggravates the pure spectral saturation component. To avoid this in future, the new IASPEI standards of amplitude measurements for m_b and m_B (cf. [42]) recommend to measure $(A/T)_{max} = A_{vmax}/2\pi$ in the entire *P*-phase train (time span *including P*, *pP*, *sP*, and possibly *PcP* and their codas but ending *preferably* before PP).

In fact the pioneers of the magnitude scales, Richter and Gutenberg, knew this, because they were still very familiar with the daily analysis of real seismic records and their complexity. Regrettably, they never wrote this down, with respect to magnitude measurements, in detail for easy reference. In the current era of automation and scientific depreciation of alleged "routine processes" the younger generation of seismologists usually had no chance to gather this experience themselves and occasionally introduced technologically comfortable but seismologically questionable practices. In an interview given in 1980 [75] Prof. Richter remembered that Gutenberg favored the body-wave scale in preference to the surface-wave scale because it is theoretically better founded. However, he said:

> "… it gives results comparable with Gutenberg's only if his procedure is closely followed. Experience has shown that misunderstanding and oversimplified misapplications can occur. For instance, magnitude is sometimes assigned on the first few waves of the *P* group rather than the largest *P* waves as Gutenberg did."

In order to avoid too-short measurement time windows when searching for the largest *P* amplitude one can estimate the rupture duration independently from the duration of large *P*-wave amplitudes in high-frequency filtered BB records because the generation of high-frequency waves is directly related to the propagation of the rupture

front. Thus one may find P_{max} for great earthquakes even beyond the theoretically expected *PP* arrival (cf. Fig. 8).

Magnitude Biases Due to Neglecting Multiple Source Complexity

Realizing that strong earthquakes usually consist of multiple ruptures Bormann and Khalturin [7] also wrote:

> "*In such cases we should determine the onset times and magnitudes of all clear successive P-wave onsets separately, as they give a first rough impression of the temporal and energetic development of the complex rupture process. … The magnitude* $MP = \log \Sigma_n(A_i/T_i) + Q(D,h)$ (*n is the number of successive P-wave onsets) could be considered as a more realistic measure of the P-wave energy released by such a multiple seismic event than the* m_b*-values from …* (single amplitude) $(A/T)_{max}$ *within the first five half cycles or within the whole P-wave group.*"

This magnitude, which is based on summed amplitudes in broadband records, is now called m_{Bc} [10], which stands for cumulative body-wave magnitude.

The 1985 $M_w = 8.1$ Mexico earthquake was a striking example for the development of such a multiple rupture process in space and time ([58], Fig. 6). A dense network of high-frequency strong-motion recordings near to the source revealed that the earthquake had a total rupture duration of about 60 s and consisted of two main subruptures with significantly increased slip-velocities (12–32 cm/s). These two fault segments were separated in space by roughly 100 km in strike direction and ruptured between 10–22 s and 34–50 s after rupture start. Such a complicated rupture is not well represented by calculating the average slip and rupture velocity for a single point-source model. Also the *corner frequencies* related to these smaller sub-ruptures will be higher and not correspond to $(L \times W)^{-1/2}$ of the total rupture area.

Such multiple ruptures are not an exception but rather the rule for earthquakes with magnitudes above 7.5 (and often also for smaller ones, even down to events with magnitudes around 5.0). The detailed patterns of the respective moment-rate curves differ from event to event (Fig. 7). Often they can not be approximated by a single-source triangular moment-rate function, as commonly assumed in the standard procedure for moment tensor solutions practiced at Harvard [78] and other centers.

Therefore, the Harvard group [78] re-analyzed the data of the great Sumatra 2004 earthquake for which $M_w = 9.0$ had been calculated with the standard procedure. Interactively fitting synthetic records for five successive point sources to the observed mantle surface-wave data in the 200–500 s period range yielded the same value of $M_w = 9.3$ as derived by [76] for a single-source model but using much longer periods between 20 min and 54 min. In fact, the multiple Centroid Moment Tensor (CMT) source analysis applied in [78] resembles the concept proposed in [7] for *P*-wave magnitudes of strong earthquakes, but applied to long-period surface waves. Presently, a multiple CMT source analysis still requires human interaction and takes too much time for early warning applications. Possible alternative procedures such a the automatic line source inversion [21] have been developed but demonstrated so far only for earthquakes with magnitudes < 7 for which classical m_B, M_S or M_w do not saturate due to source complexity.

Proposals for Faster Magnitude Estimates of Strong Earthquakes

Soon after the great Sumatra earthquake of 2004 several authors suggested improvements to obtain more reliable and faster magnitude estimates of strong earthquakes. Menke and Levin [59] proposed to use a representative selection of 25 globally distributed high quality stations of the IRIS (Incorporated Research Institutions for Seismology) Global Seismic Network as a reference data base of available strong long-period master-event records with known M_w. In case of a new strong earthquake, a search for the nearest (within a few hundred kilometers) reference event in the data base is performed and waveforms are compared for a time window of about 30 min. By adding the $\log_{10}$ of the average amplitude ratio of the two events to the M_w of the master event, a moment magnitude estimate of the actual event is obtained. This procedure is based on the assumption of similarity of *source mechanisms* and radiation patterns, slip rates and stress drops, at least within the reference regions. The authors expect reasonably good magnitude estimates, with only small underestimation for events with $M_w > 8.6$. Thus warnings could be issued within about 40 min after OT (measurement time window plus travel-time to stations of a global network). This would still be relevant for distant coasts that might be affected by a tsunami. However, no data have been published until now that demonstrate the near-real-time operational capability of this procedure for a representative set of strong events.

Another approach by Lomax et al. [55,56,57] uses high-frequency seismograms ($f \geq 1$ Hz) that contain predominantly *P* signals radiated directly from the propagating rupture front and show little interference with later

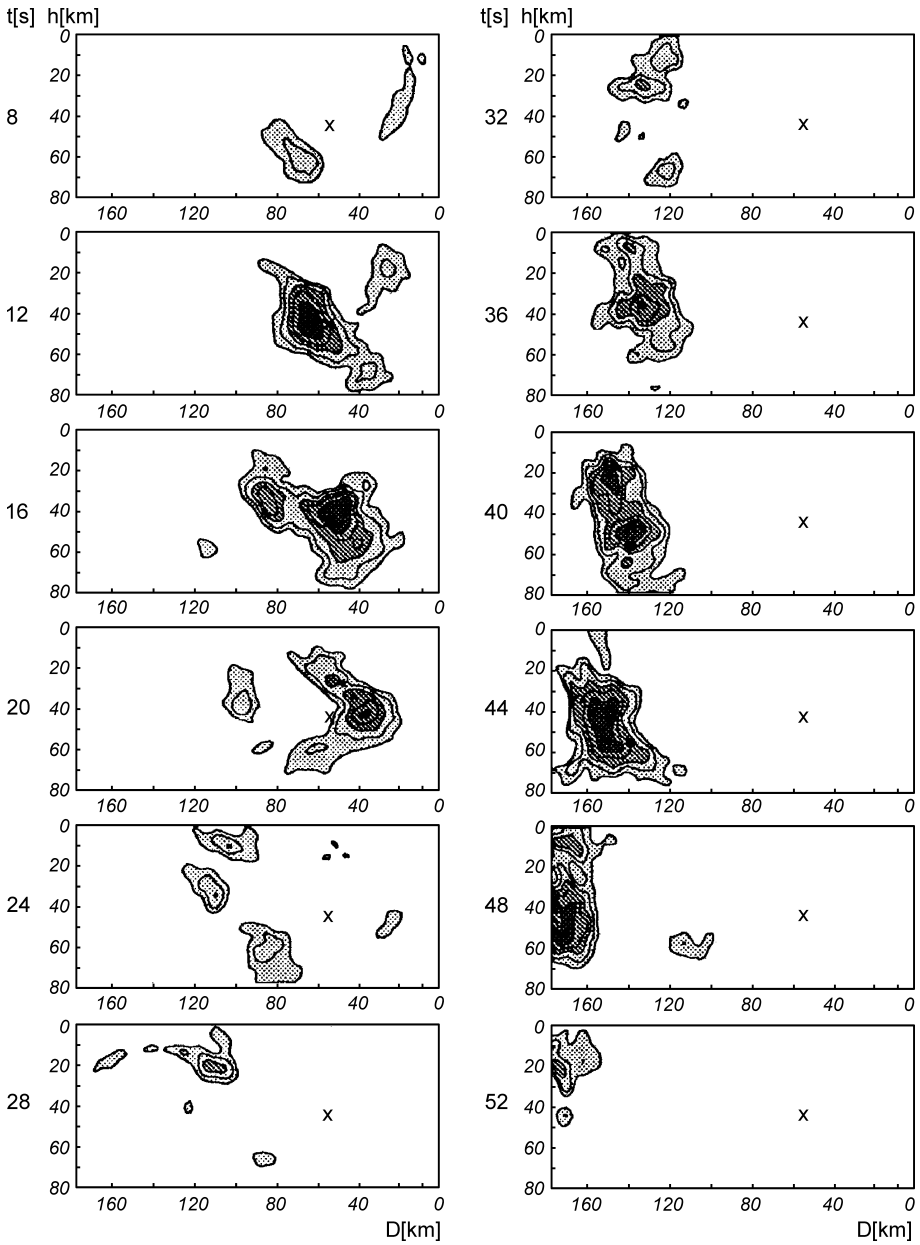

Earthquake Magnitude, Figure 6

Snapshots of the development in space and time of the inferred rupture process of the 1985 Michoácan, Mexico earthquake. The cross denotes the NEIC hypocenter position, the shading of the patches (from the outer part inwards *dotted*, *hatched* and *black*) relate to areas with velocities of dip slip (see *source mechanism*) in the ranges between 12 and 22 cm/s, 22 and 32 cm/s and greater than 32 cm/s. Redrawn and modified from Fig. 6 in [58]; taken from Fig. 3.8 in Vol. 1 of [6], © Seismological Society of America and IASPEI; with permission of the authors

secondary waves such as *PP* or *S*, thus providing a direct estimate of the rupture duration. Such recordings are available at teleseismic distances (30°–90°) within about 20 min after OT, even after strong events with long durations and provide an early picture of the total rupture process. When assuming constant rupture velocity and mean slip for stronger and weaker earthquakes, the seismic moment M_o and thus moment magnitude M_w could be estimated by comparing the actual rupture duration (averaged from observations at several seismic stations) with that of

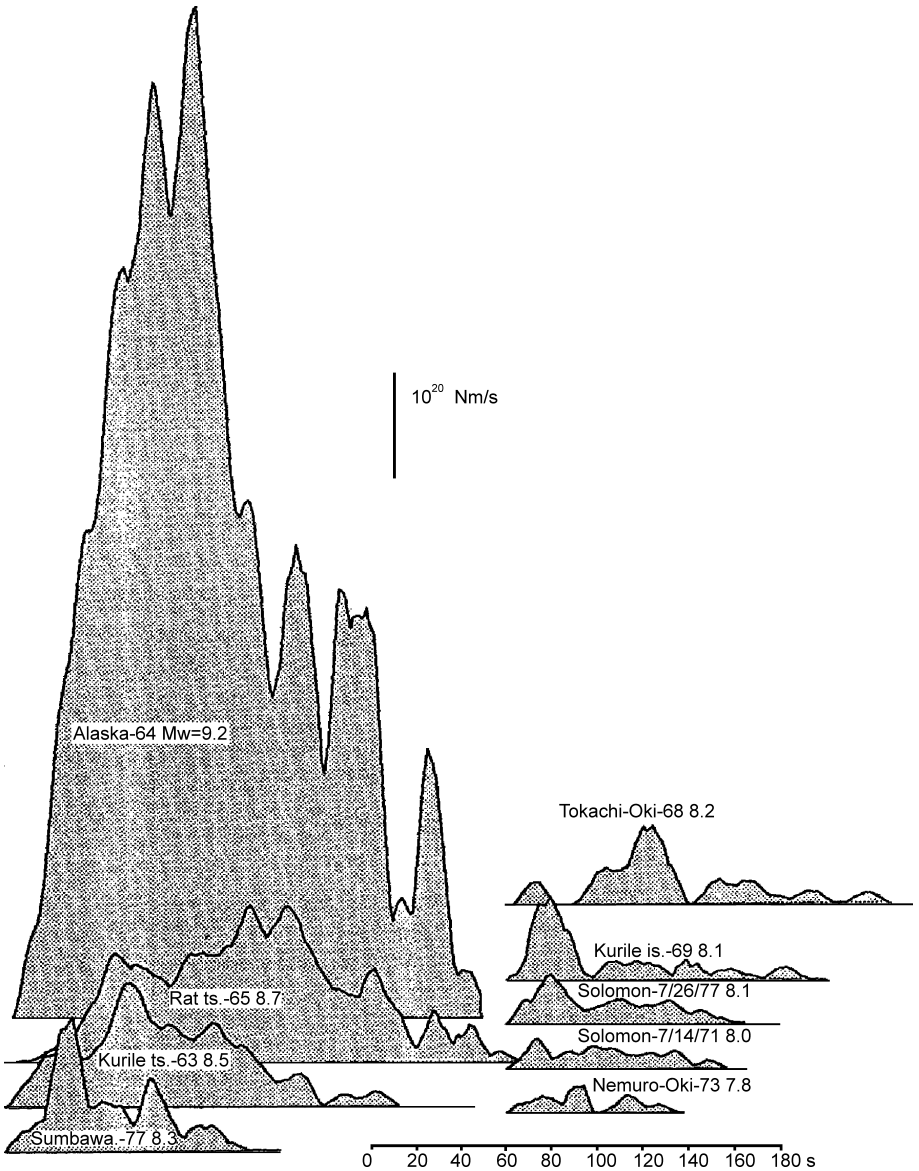

Earthquake Magnitude, Figure 7
Moment-rate functions for the largest earthquakes in the 1960 and 1970s (modified from Fig. 9, p. 1868 in [53]), taken from Fig. 3.7 in Vol. 1 of [6], © Seismological Society of America and IASPEI; with permission of the authors

a reference event with known M_o and rupture duration. This is conceptually similar to the approach in [59] but with high-frequency observations and the ratio of rupture duration instead of amplitudes.

However, Hara [32] demonstrated with a large data set of strong earthquakes that it is difficult to estimate earthquake size reliably only from durations t of high-frequency radiation. Therefore, he measured duration t in combination with the maximum displacement amplitude A_{dmax} within this time interval and derived the following empirical relation:

$$M = 0.79 \log A_{dmax} + 0.83 \log D + 0.69 \log t + 6.47 \quad (14)$$

with A_{dmax}, D and t in units of m, km and s, respectively. He applied Eq. (14) to 69 shallow earthquakes in the magnitude range $7.2 \leqslant M_w(\text{HRV}) \leqslant 9.0$ at distances between 30° and 85° and on average got a 1:1 relation between M_w(HRV) and his magnitude with a standard deviation

of 0.18 m.u. All event estimates were within ±0.5 m.u. of M_w(HRV), with the exception of the heavily underestimated Denali/Alaska earthquake of 3 November 2002 (7.1 instead of 7.8). This is a promising and simple procedure.

Bormann and Wylegalla [9] applied the earlier proposal in [7] to recordings with a velocity passband between 40 Hz and 125 s. They interactively summed up the maximum amplitudes of all visually discernible subruptures in the recordings of several recent great earthquakes with $M_w \geqslant 8.3$, amongst them the tsunamigenic $M_w = 9.3$ Sumatra earthquake of 2004. For the latter they obtained a cumulative broadband body-wave magnitude $m_{Bc} = 9.3$ in records of just a single German station (RUE; $D = 82.5°$) at the time of the second major amplitude maximum, some 330 s after the first P onset and 18 min after OT. For three more events with magnitudes M_w 8.3, 8.4 and 8.6 they calculated m_{Bc} values of 8.4, 8.4 and 8.6, respectively, i. e., excellent agreement. Subsequently, 50 more earthquakes in the magnitude range 6 to 9 were analyzed interactively [10] with the following results:

- Average difference $m_B - M_w(\text{HRV}) = 0.00 \pm 0.27$ in the range $6.0 \leqslant M_w(\text{HRV}) < 8$. For magnitudes > 7.8–8, however, m_B tends to underestimate M_w, e. g., $m_B = 8.3$ for the Sumatra earthquake of 26 December 2004 based on the BB record of station RUE. Remarkably this m_B value is still very close to M_w, M_{wp} and M_e of the NEIC, which ranged between 8.2 and 8.5.
- The average difference $m_{Bc} - M_w(\text{HRV}) = +0.18 \pm 0.26$ in the range $6.0 \leqslant M_w(\text{HRV}) \leqslant 9.0$, i. e., m_{Bc} has a tendency to slightly overestimate M_w(HRV) on average, but not for $M_w > 8$ (see the four values above).

In [10] also first results of a fully automatic determination of m_B and m_{Bc} have been presented. The algorithm has been improved by incorporating automatic estimates of the rupture duration calculated from the envelope of the high-frequency P-wave radiation from filtered broadband records of globally distributed stations in a wide range of azimuths and source distances. In the case of strong earthquakes with long rupture duration this justifies the search for broadband P_{max} even beyond the onset of PP and to sum-up the amplitudes of major sub-ruptures over the whole rupture duration as defined above. Figure 8 gives an example for a BB record of the Sumatra earthquake of 26 December 2004. The largest P-wave amplitudes at about 80 s, 280 s and 330 s after the P onset each yield a single amplitude $m_B = 8.2$, whereas the cumulative magnitude $m_{Bc} = 9.3$ is in perfect agreement with the best moment magnitude estimates for this event.

The automatic algorithm for m_B and m_{Bc} determination has been in use since spring 2007 in the operational Indonesian prototype tsunami early warning system and yields online estimates of m_B. Before the implementation it had been tested whether the automatic procedure produces results that are comparable with those determined earlier interactively by two experienced seismogram analysts. Identical broadband records of 54 earthquakes in the magnitude range $6 \leqslant M_w(\text{HRV}) \leqslant 9$ were used for this comparison based on 138 m_B and 134 m_{Bc} values. The average difference between the interactively and automatically determined magnitudes was 0.03 and 0.02 m.u. with standard deviations of ±0.13 and ±0.19 m.u., respectively. This is in the range of other high-quality magnitude measurements. Even single station m_B and m_{Bc} estimates differed on average < 0.08 m.u. from average global network estimates based on up to hundreds of stations. Their standard deviations were $< \pm 0.25$ m.u. and decreased to ±0.10 m.u. for m_B and ±0.14 m.u. for m_{Bc} when just a few stations (between two and seven) were used to estimate the m_B and m_{Bc} event magnitudes. This documents both the reliability of the automatic procedure as well as the reliability of m_B and m_{Bc} estimates, even if derived from a few records of globally distributed high-fidelity stations. Thus, the automatic procedure is suitable for reproducibly determining the IASPEI recommended standard magnitude m_B and its proposed non-saturating extension m_{Bc} in near real-time. When using only observations in the distance range $21° \leqslant D° \leqslant 100°$ saturation-free teleseismic magnitude estimates of earthquakes with potential for strong shaking damage and tsunami generation could be made available in near real-time within about 4 to 18 min after OT, depending on epicentral distance and rupture duration.

Compared to other more theoretically based methods such as M_{wp} and M_w, the empirical $m_B - m_{Bc}$ method is free of any hypothesis or model assumptions about the rupture process (single or multiple source), type of rupture mechanism, rupture velocity, average slip and/or stress drop, complexity or simplicity of the moment-release function, etc. It just measures velocity amplitudes on the unfiltered broadband record, complex or not, sums them up over the duration of the rupture process and calibrates them with the classical empirical broadband Q_{PV} function (Fig. 2 and [30]). However, one has to consider that – in contrast to all types of moment magnitudes – m_B and m_{Bc} are not determined from the maximum long-period displacement amplitudes, but from the maximum velocity amplitudes. Therefore, m_B (for earthquakes with $M_w < 8.0$) and m_{Bc} (for earthquakes with $M_w > 7.8$) are better estimators than M_w for the seismic energy released

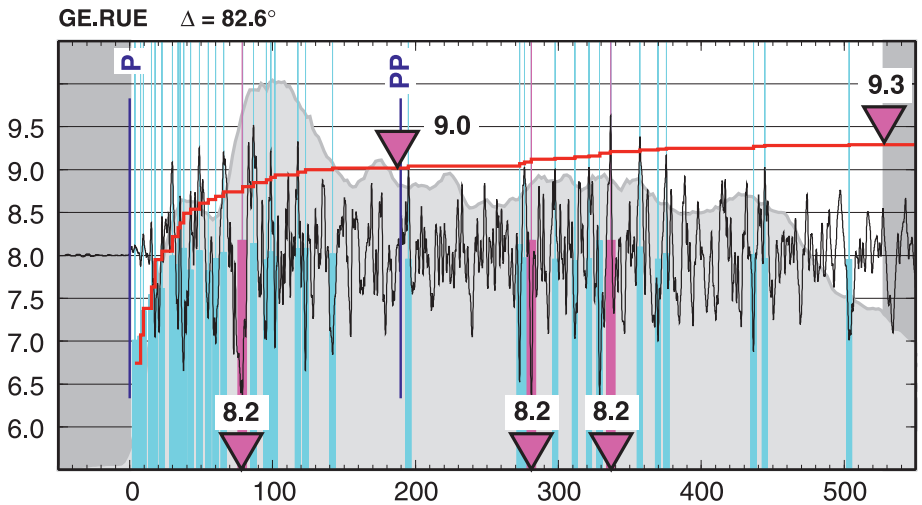

Earthquake Magnitude, Figure 8
Velocity broadband record at the Berlin station RUE in $D° = 82.6°$ epicentral distance of the great M_w9.3 tsunamigenic Sumatra earthquake of Dec. 26, 2004. The record is projected into a time-magnitude diagram as plotted by the automatic $m_B - m_{Bc}$ algorithm. The *red inverted triangles* mark the times and give the values of m_B for the three largest sub-ruptures. The *red step curve* shows the development of the cumulative magnitude m_{Bc} as a function of time. The *inverted red triangles* on this curve give the m_{Bc} before the onset of *PP* and at the end of the rupture process, about 530 s after the first *P*-wave onset, as estimated from the decay of the amplitude envelope of short-period filtered *P*-waves (see text)

by the earthquake and thus of its shaking-damage potential. Figure 9 compares m_B and m_{Bc} with M_w(HRV) for 76 earthquakes in the range $6 \leqslant M_w \leqslant 9.3$. The respective standard regression relations are:

$$M_w(\text{HRV}) = 1.22\, m_B - 1.54 \pm 0.29 \qquad (15)$$

and

$$M_w(\text{HRV}) = 1.16\, m_{Bc} - 1.59 \pm 0.25 \qquad (16)$$

These scaling relations allow much faster estimates of M_w than current routine standard M_w procedures. The rough moment estimates derived from m_B and m_{Bc} data, $M_w(m_B)$ or $M_w(m_{Bc})$, are sufficiently reliable for initial earthquake and tsunami alarms with standard deviations of the M_w estimates of about ± 0.29 and ± 0.25 m.u., respectively. However, looking into details of the somewhat irregular data scatter one realizes how *seismic source* complexity may "spoil" such regression relations. The five data points marked red in Fig. 9(left and right) are distinct outliers in the left diagram, i. e., the respective m_B values are 0.5 to 0.75 m.u. smaller than M_w(HRV) although usually m_B scales rather well with M_w(HRV) between $6.5 < m_B < 8.0$. These points correspond to slow earthquakes, one in Peru (1996) and four are tsunami earthquakes as mentioned at the end of Sect. "Common Magnitude Estimates for the Sumatra 2004 M_w 9.3 Earthquake". Their rupture durations ranged from about 100 s to 200 s, i.e, according to relationship (13) about 2–3 times longer than expected on average for their M_w value. Both m_B and M_e are usually much smaller than M_w for such events. In contrast, when calculating m_{Bc}, then these five data points all move close to the (not marked) 1:1 line in the m_{Bc}–M_w(HRV) diagram Fig. 9(right). Thus m_{Bc} becomes a good direct estimator of M_w for typical slow earthquakes, much better than via relation (16), which compensates for the usually too large m_{Bc} values of shallow depth and "normal" rupture earthquakes with $M_w < 8$. Thus, by determining rupture duration independently and treating very slow events separately, the standard deviation in relations (15) and (16) can be reduced. Moreover, the blue dots in Fig. 9 belong to very deep earthquakes with $h = 525$ km, 583 km and 631 km, respectively. Such deep earthquakes are "explosion-like" with comparably short rupture durations. Both m_B (for $M_w < 8$) and m_{Bc} yield values very close to M_w. In the m_{Bc}–M_w diagram, which is dominated by shallow and normal rupture earthquakes, such deep events appear as outliers. However, rapid event locations with good depth estimates allow one to identify such events and m_{Bc} (or m_B) should then be taken directly as estimator of M_w and not via relation (16).

M_{wp} has so far been the fastest operationally determined estimator of M_w. Comparably fast automatic m_B determination is now implemented, complementary to

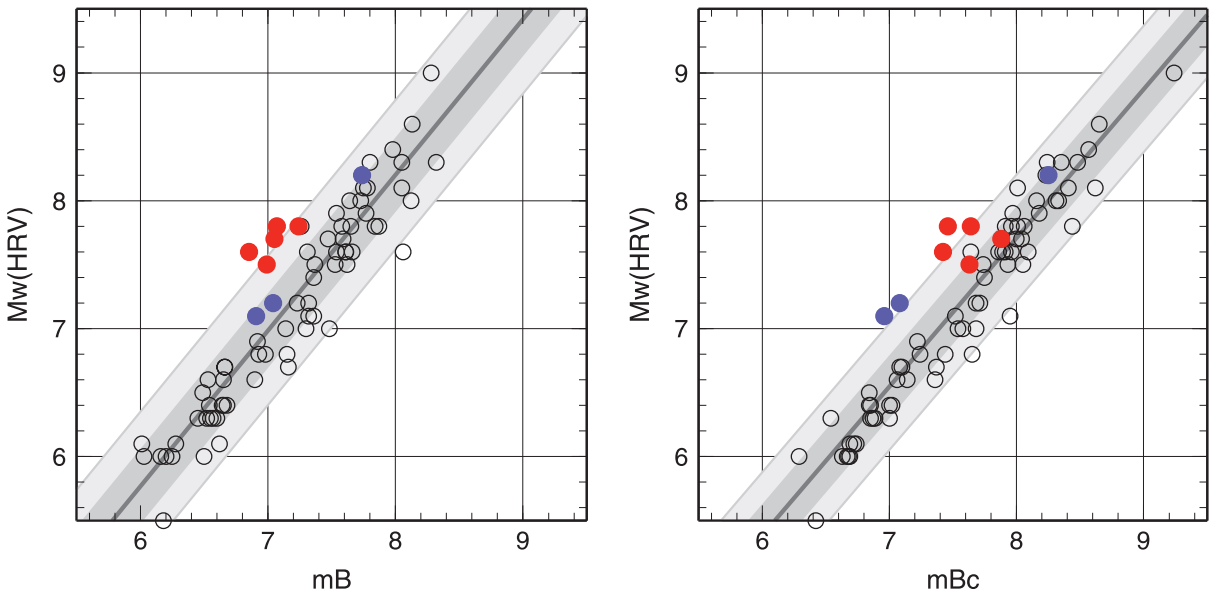

Earthquake Magnitude, Figure 9
Standard regression relationships of M_w(HRV) over m_B (*left*) and m_{Bc} (*right*). *Red dots* correspond to very slow earthquakes (Nicaragua 1992, Java 1994, New Britain Region 2000, Peru 2001 and Java 2006) and the *blue dots* belong to very deep earthquakes (Bolivia 1994, Philippines 2005 and Fiji Island 2006) with source depths $h = 631$ km, 525 km and 583 km, respectively. The *gray band* and the two *white bands* around the average *straight line* correspond to the width of one and two standard deviations in *y*-direction

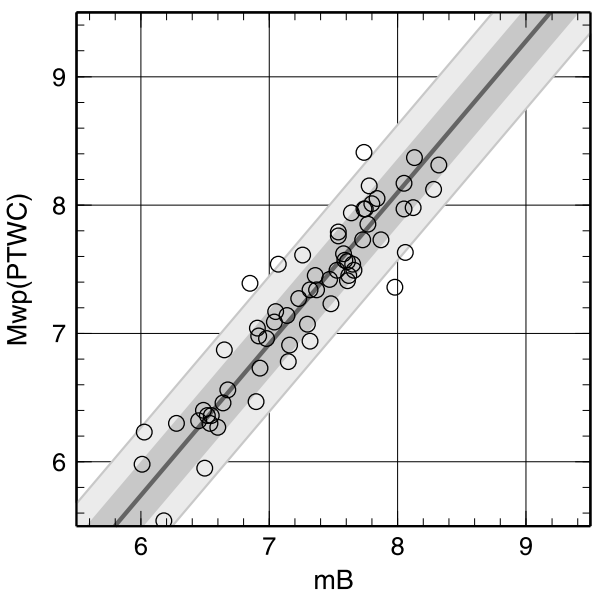

Earthquake Magnitude, Figure 10
Standard regression of M_{wp}(PTWC) over m_B. The standard deviations in *y*-direction are marked as in Fig. 9. The M_{wp} data have been kindly provided by the PTWC (courtesy of B. Hirshorn)

M_{wp}, in the German Indonesian Tsunami Early Warning System (GITEWS). Figure 10 compares the relation between m_B and M_{wp} for our test data set. These two magnitudes scale almost 1:1, following the standard regression relation:

$$M_{wp} = 1.08\, m_B - 0.638 \pm 0.24\,. \qquad (17)$$

Future Requirements and Developments

Few national seismological data centers and stations report amplitude, period and/or magnitude data to the international data centers. The main reason is usually the lack of manpower to make competent measurements of these parameters interactively for the large amount of data recorded nowadays. Instrument responses of the seismographs used are sometimes not known accurately enough. There is, however, a growing practical and research need for such parameter data that have been determined according to international standards. Therefore, the most urgent requirements in the field of magnitudes are:

- Training of station and network operators to understand and practice proper magnitude measurements, instrument calibration and control;
- Implementation of the IASPEI magnitude standards [42];
- Making the tested and calibrated automatic algorithms available worldwide to data producers so that lack of

manpower is no longer a hindrance to mass-produce such data;
- Use of such standardized mass data with significantly reduced procedure-dependent errors for improved research into the attenuation properties of the Earth and deriving better magnitude calibration functions for all distance ranges;
- Comparison of magnitude data derived from identical record sets by applying both traditional and new standard measurement procedures and to derive standardized conversion relationships. This is a precondition for assuring long-term compatibility of magnitude data in national and international data catalogs and their usefulness for seismic hazard assessment and research;
- Improvement of current procedures for direct determination of seismic moment and energy in a wider magnitude range than currently possible, down to small magnitudes that are at present well covered only by M_L and m_b;
- Development of regional calibration functions for m_b and m_B, which will permit more reliable and much faster body-wave magnitude estimates from records at distances down to about 5°
- Development and consequent use of standard procedures for M_o and E_s measurements that assure non-saturating and globally compatible estimates of seismic moment and energy and of their related magnitude scales M_w and M_e;
- Use of these data for in-depth studies in the regional variability of apparent stress conditions and their relevance for improving (time-variable) regional earthquake and tsunami hazard and risk assessment;
- Comprehensive testing of speed and reliability of the various methods recently proposed for more rapid (near) real-time magnitude estimates (e. g. [9,10,32,46, 55,56,57,59,61,66]) under operational EWS conditions;
- Development of faster automated procedures for direct non-saturating M_w and M_e determination for improving quick and realistic disaster response;
- Development of alternative automatic (near) real-time procedures of magnitude determination such as the rapid finite-source analysis [21], their scaling to both seismic energy and moment and operational testing also for very large earthquakes.

Bibliography

Primary Literature

1. Abe K (1981) Magnitudes of large shallow earthquakes from 1904 to 1980. Phys Earth Planet Int 27:72–92
2. Abe K (1984) Complements to Magnitudes of large shallow earthquakes from 1904 to 1980. Phys Earth Planet Int 34:17–23
3. Aki K (1967) Scaling law of seismic spectrum. J Geophys Res 72(4):1217–1231
4. Båth M (1981) Earthquake magnitude – recent research and current trends. Earth Sci Rev 17:315–398
5. Boatwright J, Choy GL (1986) Teleseismic estimates of the energy radiated by shallow earthquakes. J Geophys Res 91(B2):2095–2112
6. Bormann P (ed) (2002) IASPEI New manual of seismological observatory practice, vol 1 and 2. GeoForschungsZentrum, Potsdam
7. Bormann P, Khalturin V (1975) Relations between different kinds of magnitude determinations and their regional variations. In: Proceed XIVth General Ass European Seism. Comm Trieste Sept pp 16–22, 1974. Academy of Sciences of DDR, Berlin, pp 27–39
8. Bormann P, Baumbach M, Bock G, Grosser H, Choy GL, Boatwright J (2002) Seismic sources and source parameters. In: Bormann P (ed) IASPEI New manual seismological observatory practice. GeoForschungsZentrum Potsdam, chap 3, pp 1–94
9. Bormann P, Wylegalla K (2005) Quick estimator of the size of great earthquakes. EOS 86(46):464
10. Bormann P, Wylegalla K, Saul J (2006) Broadband body-wave magnitudes m_B and m_{Bc} for quick reliable estimation of the size of great earthquakes. http://spring.msi.umn.edu/USGS/Posters/
11. Bormann P, Liu R, Ren X, Gutdeutsch R. Kaiser D, Castellaro S (2007) Chinese national network magnitudes, their relation to NEIC magnitudes, and recommendations for new IASPEI magnitude standards. Bull Seism Soc Am 97(1B):114–127
12. Brune JN (1970) Tectonic stress and the spectra of shear waves from earthquakes. J Geophys Res 75:4997–5009
13. Brune JN, Engen GR (1969) Excitation of mantle Love waves and definition of mantle wave magnitude. Bull Seism Soc Am 49:349–353
14. Castellaro S, Mulargia F, Kagan YY (2006) Regression problems for magnitudes. Geophys J Int 165:913–930
15. Castellaro S, Bormann P (2007) Performance of different regression procedures on the magnitude conversion problem. Bull Seism Soc Am 97:1167–1175
16. Choy GL, Boatwright J (1995) Global patterns of radiated seismic energy and apparent stress. J Geophys Res 100, B9:18,205–18,228
17. Choy GL, Boatwright J, Kirby SH (2001) The radiated seismic energy and apparent stress of interplate and intraslab earthquakes at subduction zone environments: Implications for seismic hazard estimation. US Geological Survey Open-File Report 01–0005:18
18. Choy GL, Kirby S (2004) Apparent stress, fault maturity and seismic hazard for normal-fault earthquakes at subduction zones. Geophys J Int 159:991–1012
19. Choy GL, McGarr A, Kirby SH, Boatwright J (2006) An overview of the global variability in radiated energy and apparent stress. In: Abercrombie R, McGarr A, Kanamori H (eds) Radiated energy and the physics of earthquake faulting, AGU. Geophys Monogr Ser 170:43–57
20. Choy GL, Boatwright J (2007) The energy radiated by the 26 December 2004 Sumatra-Andaman earthquake estimated from 10-minute *P*-wave windows. Bull Seism Soc Am 97:18–24

21. Dregers DS, Gee L, Lombard P, Murray MH, Romanowicz B (2005) Rapid finite-source analysis and near-fault strong ground motions: Application to the 2003 M_w6.5 San Simeon and 2004 M_w6.0 Parkfield earthquakes. Seism Res Lett 76:40–48
22. Duda SJ (1965) Secular seismic energy release in the circum-Pacific belt. Tectonophysics 2:409–452
23. Dziewonski AM, Chou TA, Woodhous JH (1981) Determination of earthquake source parameters from waveform data for studies of global and regional seismicity. J Geophys Res 86:2825–2852
24. Ekström G, Dziewonski AM (1988) Evidence of bias in estimations of earthquake size. Nature 332:319–323
25. Geller RJ, Kanamori H (1977) Magnitudes of great shallow earthquakes from 1904 to 1952. Bull Seism Soc Am 67:587–598
26. Gutenberg B (1945) Amplitudes of P, PP, and S and magnitude of shallow earthquakes. Bull Seism Soc Am 35:57–69
27. Gutenberg B (1945) Magnitude determination of deep-focus earthquakes. Bull Seism Soc Am 35:117–130
28. Gutenberg B (1945) Amplitude of surface waves and magnitude of shallow earthquakes. Bull Seism Soc Am 35(3):3–12
29. Gutenberg B, Richter CF (1954) Seismicity of the earth and associated phenomena, 2nd Edn. Princeton University Press, Princeton
30. Gutenberg B, Richter CF (1956) Magnitude and energy of earthquakes. Ann Geofis 9:1–15
31. Hanks TC, Kanamori H (1979) A moment magnitude scale. J Geophys Res 84(B5):2348–2350
32. Hara T (2007) Measurement of duration of high-frequency energy radiation and its application to determination of magnitudes of large shallow earthquakes. Earth Planet Space 59:227–231
33. Haskell N (1964) Total energy and energy spectral density of elastic wave radiation from propagating faults, vol 1. Bull Seismol Soc Am 54:1811–1842
34. Haskell N (1964) Total energy and energy spectral density of elastic wave radiation from propagating faults, vol 2. Bull Seismol Soc Am 56:125–140
35. Hatzidimitriou P, Papazachos C, Kiratzi A, Theodulidis N (1993) Estimation of attenuation structure and local earthquake magnitude based on acceleration records in Greece. Tectonophysics 217:243–253
36. Herak M, Herak D (1993) Distance dependence of M_S and calibrating function for 20 second Rayleigh waves. Bull Seism Soc Am 83:1881–1892
37. Herak M, Panza GF, Costa G (2001) Theoretical and observed depth corrections for M_S. Pure Appl Geophys 158:1517–1530
38. Hutton LK, Boore DM (1987) The M_L scale in Southern California. Bull Seism Soc Am 77:2074–2094
39. Hyvernaud O, Reymond D, Talandier J, Okal EA (1993) Four years of automated measurements of seismic moments at Papeete using the mantle magnitude M_m: 1987–1991. In: Duda SJ, Yanovskaya TB (eds) Special section: Estimation of earthquake size. Tectonophysics 217:175–193. Elsevier Science
40. http://neic.usgs.gov./neis/sopar
41. http://www.globalcmt.org/CMTsearch.html
42. http://www.iaspei.org/commissions/CSOI/Summary_of_WG_recommendations.pdf
43. Kanamori H (1977) The energy release in great earthquakes. J Geophys Res 82:2981–2987
44. Kanamori H (1983) Magnitude scale and quantification of earthquakes. Tectonophysics 93:185–199
45. Kanamori H (1988) The importance of historical seismograms for geophysical research. In: Lee WHK (ed) Historical seismograms and earthquakes of the world. Academic Press, New York, pp 16–33
46. Kanamori H (2005) Real-time seismology and earthquake damage prediction. Ann Rev Earth Planet Sci 33:195–214
47. Kanamori H, Hauksson E, Heaton T (1997) Real-time seismology and earthquake hazard mitigation. Nature 390:461–464
48. Kanjo K, Furudate T, Tsuboi S (2006) Application of M_{wp} to the great December 26, 2004 Sumatra earthquake. Earth Planet Space 58:121–126
49. Katsumata M (1964) A method of determination of magnitude for near and deep-focus earthquakes (in Japanese with English abstract). A J Seism 22:173–177
50. Katsumata M (1996) Comparison of magnitudes estimated by the Japan Meteorological Agency with moment magnitudes for intermediate and deep earthquakes. Bull Seism Soc Am 86:832–842
51. Kaverina AN, Lander AV, Prozorov AG (1996) Global creepex distribution and its relation to earthquake – source geometry and tectonic origin. Geophys J Int 135:249–265
52. Keilis-Borok VI (1959) On the estimation of displacement in an earthquake source and of source dimension. Ann Geofis 12:205–214
53. Kikuchi M, Ishida M (1993) Source retrieval for deep local earthquakes with broadband records. Bull Seism Soc Am 83:1855–1870
54. Lee V, Trifunac M, Herak M, Živèic M, Herak D (1990) M_L^{SM} computed from strong motion accelerograms recorded in Yugoslavia. Earthq Eng Struct Dyn 19:1167–1179
55. Lomax A (2005) Rapid estimation of rupture extent for large earthquakes: Application to the 2004, M9 Sumatra-Andaman mega-thrust. Geophys Res Lett 32:L10314
56. Lomax A, Michelini A (2005) Rapid determination of earthquake size for hazard warning. EOS 86(21):202
57. Lomax A, Michelini A, Piatanesi A (2007) An energy-duration procedure for rapid and accurate determination of earthquake magnitude and tsunamigenic potential. Geophys J Int 170:1195–1209
58. Mendez AJ, Anderson JG (1991) The temporal and spatial evolution of the 19 September 1985 Michoacan earthquake as inferred from near-source ground-motion records. Bull Seism Soc Am 81:1655–1673
59. Menke W, Levin R (2005) A strategy to rapidly determine the magnitude of great earthquakes. EOS 86(19):185–189
60. Nakamura Y (1989) Earthquake alarm system for Japan railways. Jpn Railw Eng 109:1–7
61. Nakamura Y, Saita J (2007) UrEDAS, the earthquake warning system: today and tomorrow. In: Gasperini P, Manfredi G, Zschau J (eds) Earthquake early warning systems. Springer, Berlin, pp 249–281
62. Nuttli OW (1986) Yield estimates of Nevada test site explosions obtained from seismic Lg waves. J Geophys Res 91:2137–2151
63. Okal EA (1989) A theoretical discussion of time domain magnitudes: The Prague formula for M_S and the mantle magnitude M_m. J Geophys Res 94:4194–4204
64. Okal EA, Talandier J (1989) M_m: A variable-period mantle magnitude. J Geophys Res 94:4169–4193

65. Okal EA, Talandier J (1990) M_m: Extension to Love waves of the concept of a variable-period mantle magnitude. Pure Appl Geophys 134:355–384
66. Olson EL, Allen R (2005) The deterministic nature of earthquake rupture. Nature 438:212–215
67. Patton HJ (1998) Bias in the centroid moment tensor for central Asian earthquakes: Evidence from regional surface wave data. J Geophys Res 103(26):885–898
68. Polet J, Kanamori H (2000) Shallow subduction zone earthquakes and their tsunamigenic potential. Geophys J Int 142:684–702
69. Purcaru G, Berckhemer H (1978) A magnitude scale for very large earthquakes. Tectonophysics 49:189–198
70. Rezapour M, Pearce RG (1998) Bias in surface-wave magnitude M_S due to inadequate distance corrections. Bull Seism Soc Am 88:43–61
71. Richter CF (1935) An instrumental earthquake magnitude scale. Bull Seism Soc Am 25:1–32
72. Richter CF (1958) Elementary seismology. W.H. Freeman, San Francisco
73. Rydelek P, Horiuchi S (2006) Is earthquake rupture deterministic? Nature 444:E5–E6
74. Soloviev SL (1955) Classification of earthquakes by energy value (in Russian). Trudy Geophys Inst Acad Sci USSR 39(157):3–31
75. Spall H (1980) Charles F. Richter – an interview. Earthq Inf Bull 12(1):5–8
76. Stein S, Okal E (2005) Speed and size of the Sumatra earthquake. Nature 434:581–582
77. Talandier J, Okal EA (1992) One-station estimates of seismic moments from the mantle magnitude M_m: The case of the regional field ($1.5° \leqslant \Delta \leqslant 15°$). Pure Appl Geophys 138:43–60
78. Tsai VC, Nettles M, Ekström G, Dziewonski AM (2005) Multiple CMT source analysis of the 2004 Sumatra earthquake. Geophys Res Lett 32(L17304):1–4
79. Tsuboi C (1954) Determination of the Gutenberg-Richter's magnitude of earthquakes occurring in and near Japan (in Japanese with English abstract). Zisin Second Ser 7:185–193
80. Tsuboi S, Abe K, Takano K, Yamanaka Y (1995) Rapid determination of M_w from broadband P waveforms. Bull Seism Soc Am 85:606–613
81. Tsuboi S, Whitmore PM, Sokolovski TJ (1999) Application of M_{wp} to deep and teleseismic earthquakes. Bull Seism Soc Am 89:1345–1351
82. Uhrhammer RA, Collins ER (1990) Synthesis of Wood-Anderson seismograms from broadband digital records. Bull Seism Soc Am 80:702–716
83. Utsu T (2002) Relationships between magnitude scales. In: Lee WHK, Kanamori H, Jennings PC, Kisslinger C (eds) International Handbook of earthquake and engineering seismology, Part A. Academic Press, Amsterdam, pp 733–746
84. Vanek J, Zátopek A, Kárnik V, Kondorskaya N, Riznichenko Y, Savarenski S, Solovév S, Shebalin N (1962) Standardization of magnitude scales. Izv Acad Sci USSR, Geophys Ser, pp 108–111 (English translation)
85. Weinstein S, Okal E (2005) The mantle magnitude M_m and the slowness parameter Θ: Five years of real-time use in the context of tsunami warning. Bull Seism Soc Am 95:779–799
86. Whitmore PM, Tsuboi S, Hirshorn B, Sokolowski TJ (2002) Magnitude-dependent correction for M_{wp}. Sci Tsunami Hazard 20(4):187–192
87. Willmore PL (ed) (1979) Manual of seismological observatory practice, World data center A for solid earth geophysics. Report SE–20. Boulder, Colorado
88. Wu Z (2001) Scaling of apparent stress from broadband radiated energy catalogue and seismic moment catalogue and its focal mechanism dependence. Earth Planets Space 53:943–948
89. Wu KM, Kanamori H (2005) Experiment on an onsite early warning method for the Taiwan early warning system. Bull Seism Soc Am 95:347–353
90. Wyss M, Brune JN (1968) Seismic moment, stress, and source dimensions for earthquakes in the California-Nevada regions. J Geophys Res 73:4681–4694

Books and Reviews

Båth M (1979) Introduction to seismology. Birkhäuser, Basel
Bolt BA (1999) Earthquakes, 4th edn. W.H. Freeman, San Francisco
Duda S, Aki K (Eds) (1983) Quantification of earthquakes. Tectonophysics 93(3/4):183–356
Gasperini P, Manfredi G, Zschau J (eds) (2007) Earthquake early warning systems. Springer, Berlin
Kulhánek O (1990) Anatomy of seismograms. Developments in solid earth geophysics, vol 18. Elsevier, Amsterdam
Lay T, Wallace TC (1995) Modern global seismology. Academic Press, San Diego
Lee WHK (ed) (1988) Historical seismograms and earthquakes of the world. Academic Press, New York
Lee WHK, Kanamori H, Jennings PC, Kisslinger C (eds) (2002) International handbook of earthquake and engineering seismology, part A and B. Academic Press, London (an imprint of Elsevier Science)
Scholz CH (2002) The mechanics of earthquake faulting, 2nd edn. Cambridge University Press, Cambridge
Shearer PM (1999) Introduction to seismology. Cambridge University Press, Cambridge
Stein S, Wysession M (2002) Introduction to seismology, Earthquakes and earth structure. Blackwell Publishing, Malden

Earthquake Monitoring and Early Warning Systems

William H. K. Lee[1], Yih-Min Wu[2]
[1] US Geological Survey, Menlo Park, USA
[2] Department of Geosciences, National Taiwan University, Taipei, Taiwan

Article Outline